Journal of Materials Chemistry A

Accepted Manuscript

ROYAL SOCIETY OF CHEMISTRY

www.rsc.org/materialsA

Crystal structure and proton conductivity of $BaSn_{0.6}Sc_{0.4}O_{3-\delta}$: Insights from neutron powder diffraction and solid-state NMR spectroscopy

Francis G. Kinyanjui, [1,*] Stefan T. Norberg, [1] Christopher S. Knee, [1] Istaq Ahmed, [1] Stephen Hull, [2] Lucienne Buannic, [3] Ivan Hung, [4] Zhehong Gan, [4] Frédéric Blanc, [5, 6] Clare P. Grey, [3, 5] Sten G. Eriksson [1]

[1] Department of Chemical and Biological Engineering, Chalmers University of Technology, SE-412 96 Gothenburg, Sweden

[2] The ISIS Facility, STFC Rutherford Appleton Laboratory, Didcot, Oxfordshire, OX11 0QX, United Kingdom

[3] Department of Chemistry, State University of New York, Stony Brook, NY 11790-3400, USA

[4] Center of Interdisciplinary Magnetic Resonance, National High Magnetic Field Laboratory, 1800 East Paul Dirac Drive, Tallahassee, Florida 32310, United States

[5] Department of Chemistry, University of Cambridge, Lensfield Road, Cambridge, CB2 1EW, United Kingdom

[6] Department of Chemistry and Stephenson Institute for Renewable Energy, University of Liverpool, Crown Street, Liverpool, L69 7ZD, United Kingdom

* Corresponding author: Francis G. Kinyanjui

Present address:

Department of Materials,
University of Oxford,
OX1 3PH Oxford,
United Kingdom,
E-mail: francis.kinyanjui@materials.ox.ac.uk
Phone: +44 1865 612765

Abstract

The solid-state synthesis and structural characterisation of perovskite $BaSn_{1-x}Sc_xO_{3-\delta}$ (x = 0.0, 0.1, 0.2, 0.3, 0.4) and its corresponding hydrated ceramics are reported. Powder and neutron X-ray diffractions reveal the presence of cubic perovskites (space group $Pm\bar{3}m$) with an increasing cell parameter as a function of scandium concentration along with some indication of phase segregation. ^{119}Sn and ^{45}Sc solid-state NMR spectroscopy data highlight the existence of oxygen vacancies in the dry materials, and their filling upon hydrothermal treatment with D_2O. It also indicates that the Sn^{4+} and Sc^{3+} local distribution at the B-site of the perovskite is inhomogeneous and suggests that the oxygen vacancies are located in the scandium dopant coordination shell at low concentrations ($x \leq 0.2$) and in the tin coordination shell at high concentrations ($x \geq 0.3$). ^{17}O NMR spectra on ^{17}O enriched $BaSn_{1-x}Sc_xO_{3-\delta}$ materials show the existence of Sn-O-Sn, Sn-O-Sc and Sc-O-Sc bridging oxygen environments. Further room temperature neutron powder diffraction study on deuterated $BaSn_{0.6}Sc_{0.4}O_{3-\delta}$ refines the deuteron position at the 24*k* crystallographic site (x, y, 0) with x = 0.579(3) and y = 0.217(3) which leads to an O-D bond distance of 0.96(1) Å and suggests tilting of the proton towards the next nearest oxygen. Proton conduction was found to dominate in wet argon below 700 °C with total conductivity values in the range 1.8×10^{-4} to 1.1×10^{-3} S cm^{-1} between 300 and 600 °C. Electron holes govern the conduction process in dry oxidizing conditions, whilst in wet oxygen they compete with protonic defects leading to a wide mixed conduction region in the 200 to 600 °C temperature region, and a suppression of the conductivity at higher temperature.

Keywords:

Proton Conducting Electrolyte, Neutron Powder Diffraction, Solid-State NMR, Deuteron Position, $BaSnO_3$, Mixed conductor

1. Introduction

During the past three decades proton conducting ceramics have been widely studied due to their high ionic conductivities in the intermediate temperature region of 300-600 °C. In particular these materials have been proposed to be used as proton conducting electrolytes in protonic ceramic fuel cells (PCFC). The lower operating temperature of PCFCs would provide substantial advantages over solid oxide fuel cells (SOFC) based on oxide ion-conducting electrolytes. The higher operating temperatures of SOFCs, usually 700-900 °C, has limited its technological development due to high system costs, performance degradation rates, slow start-up and shutdown cycles. For example, in the 700-900 °C temperature range, the use of chromium containing interconnector steels might cause chromium poisoning of the electrodes [1] and shorten the lifetime of the cell. Reduced start-up times and relaxed matching of the thermal expansion coefficients of the various fuel cell components are additional benefits that accompany the lowering of the operating temperature.

Acceptor doped perovskites provide many eligible systems for proton conducting electrolytes, e.g. $BaZr_{1-x}Y_xO_{3-\delta}$ [2-4], $BaCe_{1-x}Y_xO_{3-\delta}$ [2], $SrCe_{1-x}Y_xO_{3-\delta}$ [5], $BaZr_{1-x}Yb_xO_{3-\delta}$ [6] all with $0 \leq x \leq 0.2$, and $BaZr_{1-x}In_xO_{3-\delta}$ [7] with $0 \leq x \leq 1$. Below 700 °C, $BaZr_{1-x}Y_xO_{3-\delta}$ possesses a bulk conductivity greater than the best oxide ion conductors [2]. Proton incorporation is reliant on the formation of oxygen vacancies in a process commonly referred to as acceptor doping in the $A^{2+}B^{4+}O^{2-}{}_3$ type perovskites. Here, a portion of the tetravalent cations at the *B*-site is substituted by trivalent dopant cations resulting in the formation of charge compensating oxygen vacancies in the system. This process can be described using Kröger-Vink notation for Sc-doped $BaSnO_3$ with Sc^{3+} doped on the Sn^{4+} site as:

$$2Sn_{Sn}^{\times} + O_O^{\times} + Sc_2O_3 \rightarrow 2Sc'_{Sn} + V_O^{\bullet\bullet} + 2SnO_2 \qquad (1)$$

with Sc'_{Sn} corresponding to a Sc^{3+} ion sitting on a Sn site with a negative charge, and $V_O^{\bullet\bullet}$ to an oxygen vacancy with two positive charges. When in contact with a H_2O bearing gas the oxygen vacancies $V_O^{\bullet\bullet}$ are filled via the following reaction:

$$H_2O_{(g)} + V_O^{\bullet\bullet} + O_O^{x} \leftrightarrows 2OH_O^{\bullet} \qquad (2)$$

with $OH_O^{\bullet}$ corresponding to a OH^- ion sitting on a O lattice site with a positive charge.

However, in oxidizing conditions and in some systems, electronic holes can instead compensate for the vacancies via the following equation leading to p-type hole ($h^{\bullet}$) conduction:

$$\tfrac{1}{2}O_2\,(g) + V_O^{\bullet\bullet} \leftrightarrows O_O^x + 2h^{\bullet} \qquad (3)$$

Under low oxygen partial pressures the following mechanism can occur yielding n-type electronic conduction:

$$O_O^x \leftrightarrows \tfrac{1}{2}O_2\,(g) + V_O^{\bullet\bullet} + 2e' \qquad (4)$$

Significant proton conduction has been reported in substituted stannate phases such as $BaIn_{0.5}Sn_{0.5}O_{2.75}$ [8], $Ba_2YSnO_{5.5}$ [9], $BaSn_{1-x}M_xO_{3-\delta}$ with M = Sc, Y, In and Gd, $x = 0.125$ [10] and x = 0.25 [11] and $BaSn_{1-x}Y_xO_{3-\delta}$ ($0 \leq x \leq 0.5$) [12]. More recently, Li and Nino reported on proton conductivity of $BaSn_{0.9}M_{0.1}O_{3-\delta}$ (M = In, Lu, Er and Y) in oxidising and reducing conditions [13], whilst Bévillon *et al.* [14] used a density functional theory approach to probe the energy landscape of the proton in substituted $BaSn_{1-x}M_xO_{3-x/2}$.

In this study, $BaSn_{1-x}Sc_xO_{3-\delta}$ was selected as the system of interest as the recent studies highlighted above have established acceptor doped $BaSnO_3$ as a promising alternative candidate to the more widely studied $BaZrO_3$ and $BaCeO_3$ systems. Scandium was chosen here as the dopant as it has an ionic radius that is only slightly larger than that of tin (0.745 Å and 0.69 Å for Sc^{3+} and Sn^{4+} respectively in 6-fold coordination) [15]. We report the preparation and characterisation of the $BaSn_{1-x}Sc_xO_{3-\delta}$ series with $0 \leq x \leq 0.4$ via PXRD and solid-state NMR techniques. The highest acceptor doped sample, $BaSn_{0.6}Sc_{0.4}O_{3-\delta}$, was selected for detailed study as it shows the largest incorporation of scandium, and thus, in principle, is expected to possess the highest proton concentration on hydration. While the location of the oxygen vacancies was determined by ^{119}Sn, ^{45}Sc, and ^{17}O multinuclear solid-state NMR spectroscopy by investigating the presence of Sn and Sc cations with various coordination numbers, the position of the deuteron ions in D_2O treated $BaSn_{0.6}Sc_{0.4}O_{3-\delta}$ was found by neutron powder diffraction (NPD). Finally, the electrical conductivity was studied using

electrochemical impedance spectroscopy (EIS) recorded under different atmospheres to reveal the temperature dependence of the dominating charge carriers.

2. Experimental

2.1. Synthesis

$BaSn_{1-x}Sc_xO_{3-\delta}$ with x = 0, 0.1, 0.2, 0.3 and 0.4 were synthesized by a solid state reaction using stoichiometric amounts of $BaCO_3$ (Merck 99%), SnO_2 (Sigma-Aldrich 99.9%), and Sc_2O_3 (Sigma-Aldrich 99.9%). The reactants were weighed and finely mixed to a paste using a mortar and pestle and ethanol before heating at 1000 °C for 8 h. The powders were then ball milled to a fine powder for 8 h in a Teflon milling house with ethanol using a planetary ball mill and zirconium milling balls. The powders were then dried and pressed into pellets, and subsequently reacted at 1200 °C for 72 h before being ball milled, pelletized and heated again at 1455 °C for 24 h. The sintered pellets were thereafter milled into a fine powder to give the as-prepared samples. All the heating steps were performed under an oxygen gas flow.

Hydration of $BaSn_{1-x}Sc_xO_{3-\delta}$ was performed by heating the powders with a stoichiometric amount of D_2O, calculated to correspond to the complete filling of oxygen vacancies, in a hydrothermal bomb at 225 °C for 12 h. Drying of samples for NMR and NPD measurements was performed by treating at 900 °C for 8 h under vacuum. ^{17}O NMR data were collected on samples that have been enriched in ^{17}O by heating the freshly dried samples (1 h at 950 °C under vacuum) under 50 % ^{17}O enriched O_2 gas (Isotec, 99 %) for 2 days at 950 °C.

Conductivity measurements on a sample of $BaSn_{0.6}Sc_{0.4}O_{3-\delta}$ were performed on a 16 mm diameter, 72 % dense pellet (made by uni-axially pressing of powders at 8 tons) which was sintered at 1455 °C for 24 h. The pellet was then coated on both faces with platinum paste, heated for 2 h at 1000 °C to remove the organic component of the paste, and finally, treated for 7 days in a furnace at 300 °C with a vapour saturated N_2 gas flow ($p(H_2O) \approx 0.40$ atm) to give a pre-hydrated sample.

2.2. X-ray powder diffraction (PXRD)

PXRD data for the as-prepared samples were collected on a Bruker AXS D8 ADVANCE VARIO X-ray powder diffractometer ($CuK_{\alpha 1}$= 1.54058 Å) equipped with a LynxEye detector and a germanium (111) primary monochromator. The step size used was 0.050 ° with a collection time of 0.7 s per step in the 27° to 72° 2-theta range.

2.3 Neutron Powder Diffraction (NPD)

NPD data were collected at room temperature on dried $BaSnO_3$, dried $BaSn_{0.6}Sc_{0.4}O_{3-\delta}$ and D_2O treated $BaSn_{0.6}Sc_{0.4}O_{3-\delta}$ samples using the Polaris [16] instrument at the ISIS neutron facility, and subsequently analysed using the GSAS [17, 18] software package. Data from two detector banks were used for the structure refinements, i.e. the backscattering detector bank (covering scattering angles of $130° < 2\theta < 160°$, and a *d*-spacing range of $0.2 < d$ (Å) < 3.2, with a resolution of $\Delta d/d \sim 5 \times 10^{-3}$), and the 90° detector bank ($85° < 2\theta < 95°$; $0.3 < d$ (Å) < 4.1; $\Delta d/d \sim 7 \times 10^{-3}$). Data were collected for approximately 9 h for the D_2O treated $BaSn_{0.6}Sc_{0.4}O_{3-\delta}$ sample and 1 h for the dried samples.

Rietveld refinements [18-20] included the following parameters: a scale factor, the cubic lattice parameter *a*, background parameters describing a reciprocal interpolar function, isotropic thermal vibration parameters for the cation sites, u_{Ba}, $u_{Sn/Sc}$, and anisotropic parameters for the oxygen site, u_{11}, u_{22}=u_{33} and 4 profile parameters describing Gaussian and Lorentzian contributions to the Bragg peak profiles in the cubic space group $Pm\bar{3}m$. Ba was set at 1*b* (½, ½, ½), Sn/Sc at 1*a* (0, 0, 0) and O at 3*d* (½, 0, 0). Ahmed *et al.* [21] reported the likelihood of the deuteron being located at the 24*k* (0.55, 0.20, 0) crystallographic site for $BaZr_{0.5}In_{0.5}O_{2.5}(OD)_{0.5}$ and this was used as a starting point in the analysis of the data from the deuterium containing sample.

2.4. Solid-State NMR

^{119}Sn NMR spectra were acquired at 11.7 T on a wide bore Oxford 500 MHz Varian Infinity Plus spectrometer using a 3.2 mm HX Chemagnetics probehead tuned to 186.26 MHz. The $BaSnO_3$ (dried) and $BaSn_{0.6}Sc_{0.4}O_{3-\delta}$ samples (in vacuum dried and D_2O treated forms) were packed under

nitrogen gas atmosphere in 3.2 mm zirconia rotors, which were then spun at a spinning frequency ν_r = 20 kHz. ^{119}Sn single pulse experiments were carried out using a $\pi/2$ pulse width of 2 μs (*i.e.* at an r.f. field amplitude of ν_1^{Sn} = 125 kHz) and a recycle delay of 70 s allowing full relaxation of the ^{119}Sn spins. Chemical shifts were externally referenced to SnO_2 at -604.3 ppm.

High field ^{45}Sc NMR experiments were performed at 19.6 T on a ultra-narrow bore Bruker DRX 830 MHz spectrometer at the National High Magnetic Field Laboratory, Tallahassee, Florida, USA using a home-built 1.8 mm single channel probe [22] tuned to 202.44 MHz. All samples were packed inside 1.8 mm rotors, spun at a spinning frequency ν_r of 33.333 kHz, and short recycle delays of 0.2 s allowing full relaxation of the ^{45}Sc spins were used for the 1D spectra. t_1 rotor synchronized two-dimensional (2D) triple-quantum MAS (TQMAS) experiments [23-25] were performed using a shifted-echo pulse sequence and the Soft-Pulse-Added-Mixing (SPAM) enhancement pulse [26]. Hard and soft pulses were performed at radio-frequency (*rf*) field amplitudes of ν_1^{Sc} = 150 kHz and approximately ν_1^{Sc} = 20 kHz, respectively. Chemical shifts were externally referenced to a 1 M solution of $Sc(NO_3)_3$ in water at 0.0 ppm.

^{17}O NMR experiments were carried out on a 17.6 T wide bore Bruker Avance 750 MHz spectrometer equipped with a 4 mm HXY (in double resonance mode) probehead and operating at 101.72 MHz. All samples were packed inside 4 mm rotors and spun at a spinning frequency ν_r of 15 kHz. ^{17}O one-dimensional spectra were recorded using a one pulse sequence with selective pulse widths of $\pi/6$ = 0.6 μs and at an rf field amplitude of ν_1^{O} = 50 kHz. t_1 rotor synchronized two-dimensional (2D) TQMAS experiments were performed using the z-filtered pulse sequence [27]. Hard and soft pulses were performed at *rf* field amplitudes of ν_1^{O} = 50 kHz and approximately ν_1^{O} = 10 kHz, respectively. The recycle delays were set to 5 s for all experiments. Chemical shifts were externally referenced to water at 0.0 ppm.

All data were processed with MatLab and MatNMR [28].

2.5. Impedance Spectroscopy

A ProboStat™ (NorECs AS, Norway) cell coupled to a Solartron 1260 frequency response analyser in standalone mode were used to collect electrochemical impedance data. Data collection was between 1 Hz and 1 MHz at 1 V rms amplitude between 150 and 1000 °C in steps of 50 °C with an equilibration time of 30 minutes before data collection. Data was collected for $BaSn_{0.6}Sc_{0.4}O_{3-\delta}$ in the following sequence: pre-hydrated sample heating and cooling in dry Ar gas, wet (humidified) Ar gas cooling, wet O_2 gas on cooling, and finally dry O_2 gas on cooling. Two silica tubes, one inside the other, were used to cover the cell, and two P_2O_5 gas traps before the cell were used to ensure dry gas conditions within the cell. A dense mullite–alumina tube was used in conjunction with a water bubbler at ambient temperature to provide wet gas ($p(H_2O) \approx 0.025$ atm) within the cell.

3. Results

3.1. X-ray Diffraction

Figure 1 shows the PXRD pattern for all dried $BaSn_{1-x}Sc_xO_{3-\delta}$ samples (x = 0.0, 0.1, 0.2, 0.3 and 0.4). These data reveal that all samples are highly crystalline and the patterns indicate that the phases adopt a cubic perovskite structure (space group $Pm\bar{3}m$) across the range of compositions. The cell parameters, obtained from profile fitting using Jana2006 [29], increased with increase of dopant fraction in agreement with the Sc^{3+} ionic radius (0.745 Å) being larger than Sn^{4+} (0.69 Å) [15]. Close inspection of the data revealed evidence of peak shoulders at $2\theta \approx 44°$, 54° for the x = 0.1, 0.2 and 0.3 samples. This behaviour was rationalised in terms of phase segregation into $BaSnO_3$ and a $BaSn_{1-x}Sc_xO_{3-\delta}$ phase comparatively rich in scandium in order to preserve the overall stoichiometry of the initial sample reactants. This behaviour was not apparent for the x = 0.4 sample, and its cell parameter of 4.1367(1) Å showed a significant enlargement compared to the value of 4.1156(1) Å determined for un-doped $BaSnO_3$. $BaSn_{0.6}Sc_{0.4}O_{3-\delta}$, which showed the highest incorporation of scandium based on the PXRD results, was therefore selected for further study via neutron diffraction and impedance measurements.

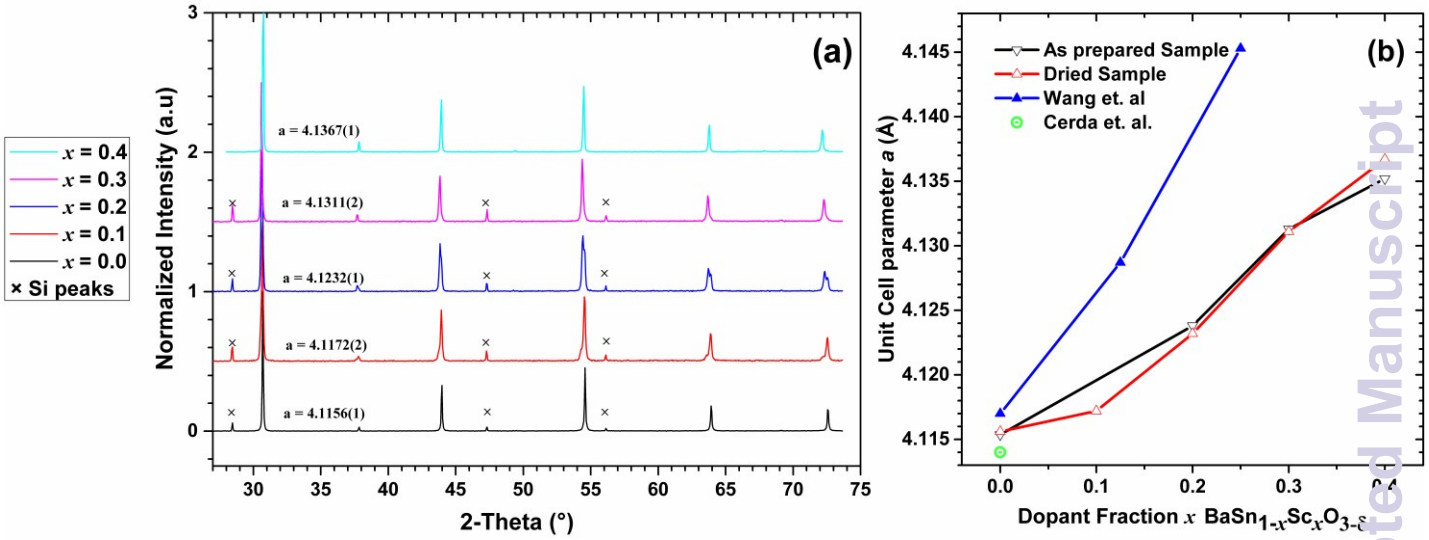

Figure 1 a) PXRD patterns collected on dried $BaSn_{1-x}Sc_xO_{3-\delta}$ samples with the indicated cell parameters in Ångstroms. b) Comparison of the cell parameters for the dried and as prepared $BaSn1_{-x}Sc_xO_{3-\delta}$ samples with values reported by Wang et al,[10, 11] and Cerda et al[30]

3.2. Neutron Diffraction

The NPD data for $BaSn_{0.6}Sc_{0.4}O_{3-\delta}$ presented in Figure 2 revealed that a minor Sc_2O_3 impurity phase was present in the vacuum dried sample. The large neutron scattering lengths of scandium (12.29 fm) and oxygen (5.803 fm) compared to their relatively weaker X-ray scattering powers could explain why this minor phase was detected in the neutron pattern (Figure 2) but was not visible in the PXRD patterns (Figure 1). The Sc_2O_3 peaks are not visible in the NPD of deuterated $BaSn_{0.6}Sc_{0.4}O_{3-\delta}$ where only a single, deuteron containing, perovskite phase is present.

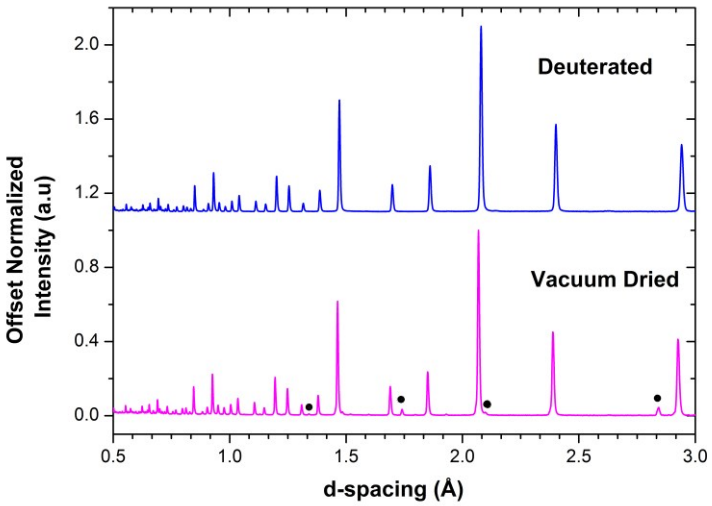

Figure 2 NPD patterns of vacuum dried and deuterated $BaSn_{0.6}Sc_{0.4}O_{3-\delta}$. Black filled circles indicate reflections arising from a small amount of Sc_2O_3.

3.2.1 Vacuum Dried $BaSn_{0.6}Sc_{0.4}O_{3-\delta}$:

As starting models three phases namely, $BaSn_{0.6}Sc_{0.4}O_{2.8}$ and $BaSnO_3$, both modelled using the cubic $Pm\bar{3}m$ crystal system, and Sc_2O_3 were included into the Rietveld analysis of the dried sample, Phase 1, 2 and 3 respectively. The weight fractions of these three phases obtained from the refinement were 95.55(1) wt%, 3.34(8) wt% and 1.11(1) wt%, respectively (Figure S1). The Sn:Sc site occupancy in the dominant perovskite phase 1 was reciprocally linked and refined to give a small increase in the Sn:Sc ratio, with 0.666(2) and 0.334(2) site occupancies for Sn and Sc, respectively. The overall sample stoichiometry was consistent with the initial 0.6 Sn and 0.4 Sc molar fractions. Modelling the oxygen atoms with an anisotropic displacement parameter (ADP) significantly reduced the values of the χ^2 goodness of fit parameter from 15.66 to 10.86. Simultaneous refinement of the oxygen ADP and occupancy was not deemed reliable due to the high degree of correlation between these two variables. Hence the occupancy of the oxygen site in phase 1 was set to 0.944 as would be expected for a dried sample with a $BaSn_{0.666}Sc_{0.334}O_{3-\delta}$ composition with a final χ^2 value of 6.372.The final agreement to the data is shown in the supplementary data (Figure S1). Note that for simplicity

we continue to refer to this sample as $BaSn_{0.6}Sc_{0.4}O_{3-\delta}$, despite the slightly lower Sc content of the perovskite phase.

3.2.2 Hydrothermally D_2O treated $BaSn_{0.6}Sc_{0.4}O_{3-\delta}$:

Given the absence of additional impurity reflections, the Sn^{4+} and Sc^{3+} occupancies used in the Rietveld fit to the NPD data were fixed to the nominal values of 0.6 and 0.4, respectively, for D_2O treated $BaSn_{0.6}Sc_{0.4}O_{3-\delta}$. The occupancy of the oxygen and barium sites was permitted to vary and both favoured a value slightly above unity and were therefore set to one. This is consistent with complete filling of oxygen vacancies by OD groups as per equation 2 above during the hydrothermal treatment with D_2O. The fit improved significantly by allowing the oxygen ADP factor to vary anisotropically. The deuteron position was investigated by Rietveld analysis and the use of Fourier difference maps as described previously [21]. Missing positive scattering was observed near fractional coordinates $x = 0.55$, $y = 0.2$ and $z = 0.0$, *i.e.* the crystallographic 24*k* site. The deuteron site occupancy was calculated from the number of filled oxygen vacancies with respect to the refined oxygen occupancy, *e.g.* $BaSn_{0.6}Sc_{0.4}O_{2.6}(OD)_{0.4}$, which corresponds to a 24*k* site occupancy of ~ 0.017. The isotropic ADP parameter was then set free to refine together with the atomic coordinates *x* and *y* of the deuteron at the 24*k* site. This resulted in a significant reduction in the standard uncertainties of the refined parameters and a small reduction in the goodness of fit parameters. The deuteron positional coordinates (*x*, *y*, 0) refined to (0.579(3), 0.217(3), 0). Results of the Rietveld analysis of the NPD data are listed in Table 1, and the final Rietveld fit achieved is shown in Figure 3.

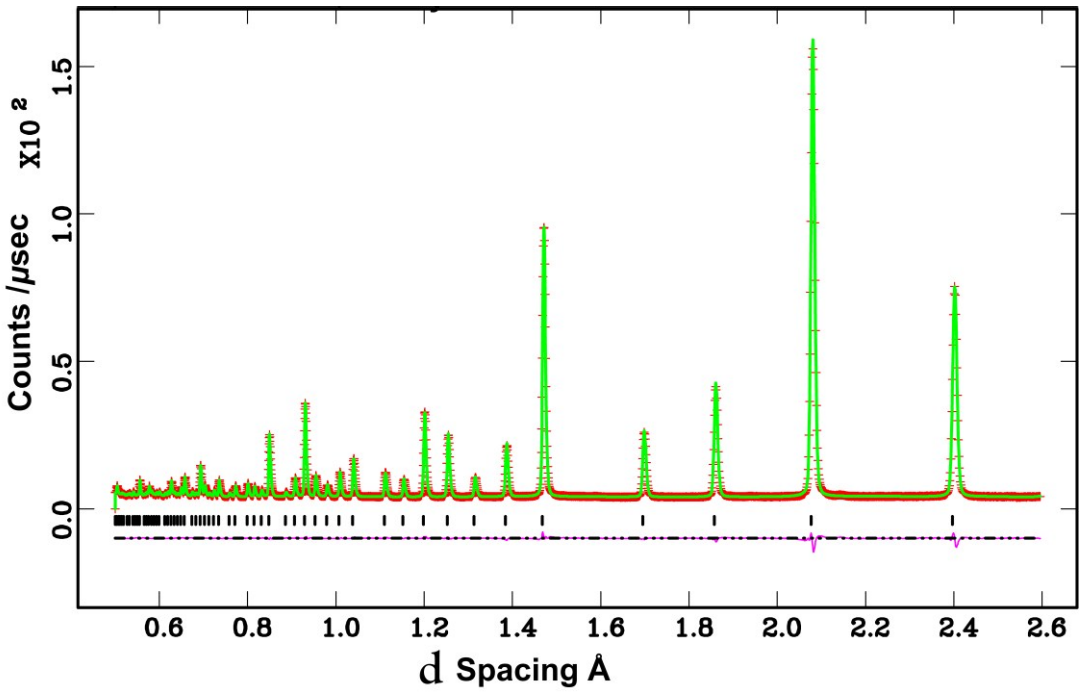

Figure 3 Rietveld fit to the data for $BaSn_{0.6}Sc_{0.4}O_{2.6}(OD)_{0.4}$ with the deuteron modelled at the 24*k* site. Both the observed (red crosses) and calculated (continuous green line) profiles are plotted and the position of the reflections is marked with vertical black bars. The difference curve lies at the bottom in purple.

Table 1. Refined parameters from neutron powder diffraction of dried $BaSnO_3$ and both dried and deuterated $BaSn_{0.6}Sc_{0.4}O_{3-\delta}$.

Refinement parameters	dry $BaSnO_3$	$BaSn_{0.6}Sc_{0.4}O_{3-\delta}$	
		dry	deuterated
a (Å)	4.11588(2)	4.13549(1)	4.15716(2)
U_{iso} (Å^2) *100			
Ba	0.416(4)	0.614(5)	1.2 00(5)
Sn/Sc	0.231(3)	0.712(6)	1.057(4)
O U_{11}	0.294(8)	0.334(11)	0.498(8)
O U_{22}-U_{33}	0.923(6)	1.201(7)	1.261(5)
D (*x*, *y*, 0)			0.579(3), 0.217(3), 0
D (*x*, *y*, 0) U_{iso}			11.3(4)
Occupancy			
Ba (0.5, 0.5, 0)	1.0 [a]	1.0 [a]	1.0 [a]
Sn (0, 0, 0)	1.0 [a]	0.666(2)	0.6
Sc (0, 0, 0)	-	0.334(2)	0.4
O (0.5, 0, 0)	1.0	0.944 [b]	1.0 [a]
D (*x*, *y*, 0)	-	-	0.0167 [c]
Bond distances (Å)			
12 × Ba-O	2.91037(1)	2.92423(1)	2.93956(1)
6 × Sn/Sc-O	2.05794(1)	2.06774(1)	2.07858(1
1× O-D			0.959(12)
1× O-D$^{(1-y, x, z)}$			2.109(7)
1× O-D$^{(-y, x, z)}$		-	2.680(6)
2× O-D$^{(1+z, y, -x)}$			2.862(9)
χ^2	48.16	6.37	12.84
R_{wp} (%)	0.0314	0.0283	0.0124
R_p (%)	0.0360	0.0441	0.0169
Phases (wt. %)			
Main	100	95.55(1)	100
Sc_2O_3	-	1.11(1)	-
$BaSnO_3$	-	3.34(8) [d]	-
Variables	-	26	47

[a] Occupancies refined to slightly larger than 1, and therefore fixed to 1.
[b] Due to correlation between the oxygen site ADP and occupancy this value was not refined in final stages, instead it was fixed to the value determined by the amount of refined scandium x = *0.334* (Oxygen fraction = (3-(*0.334*/2))/3 .
[c] Occupancy of the deuterium site was fixed to reflect a deuterium content consistent with complete filling of the oxygen vacancies.
[d] The refined unit cell parameter was 4.11457(17) Å.

3.3 Solid-State NMR

3.3.1 ^{119}Sn NMR

The ^{119}Sn magic angle spinning (MAS) NMR spectrum of dry $BaSnO_3$ (Figure S2a in the Supplementary Information) shows a sharp resonance at –679 ppm corresponding to tin in a six-fold symmetrical environment [31]. This environment corresponds to Sn surrounded by 6 tin atoms in its first cation coordination shell, giving rise to a $Sn(OSn)_6$ local environment [31], the only chemical environment in the undoped $BaSnO_3$ material.

In dry Sc-substituted $BaSnO_3$, a new set of ^{119}Sn resonances with intensity proportional to Sc concentration appears at around –640 ppm (Figure 4a). This feature is assigned to tin in six fold environments surrounded by at least one scandium cation based on previous NMR studies of the related Y-doped $BaSnO_3$ materials [32]. In this system, the six-coordinated Sn cations with various numbers of Y ions in their first cationic coordination shells, *i.e.* $Sn(OSn)_5(OY)$, $Sn(OSn)_4(OY)_2$, $Sn(OSn)_3(OY)_3$, etc. could be individually observed, the ^{119}Sn resonance shifting by +27 to +34 ppm per added Y ion. Here the ^{119}Sn spectra of Sc-doped $BaSnO_3$ lacks such sharp, resolved features, most likely due to a smaller frequency shift per Sc ion added to the vicinity of the Sn nuclei. Indeed the ionic radius of Sc^{3+} in 6-fold coordination (0.745 Å) is much closer to the one of Sn^{4+} (0.69 Å) in comparison to Y^{3+} (0.90 Å) leading to smaller local distortions in the case of Sc substitution and therefore smaller frequency shifts. A weak but sharp $BaSnO_3$ resonance is seen in all four samples (x = 0.1, 0.2, 0.3 and 0.4) at –679 ppm most likely due to a separate $BaSnO_3$ impurity phase; the weakest $BaSnO_3$ resonance was seen for x = 0.4, consistent with the low phase fraction obtained in the NPD refinement of this phase (Figures 2 and S1).

A second broad resonance, centered at –450 ppm (Figure 4a), is assigned to five-coordinated Sn environments in line with a shift to higher frequency going from six to five-fold Sn coordination [31, 32], a trend generally observed for a number of nuclei [33].

On hydrothermal D_2O treatment of dry $BaSn_{1-x}Sc_xO_{3-\delta}$ (Figure 4b), the ^{119}Sn NMR resonance at –450 ppm, associated with the five-coordinated Sn environments, totally disappears, which is consistent with its assignment, and shows complete reaction of the oxygen vacancies $V_O^{\bullet\bullet}$ with D_2O during hydration to form six-coordinated Sn environments (experimentally observed at –636 ppm). The sharp –679 ppm resonance is also seen, providing evidence for $BaSnO_3$ environments although no sign of an impurity phase was detected in the NPD data, presumably due to its low concentration.

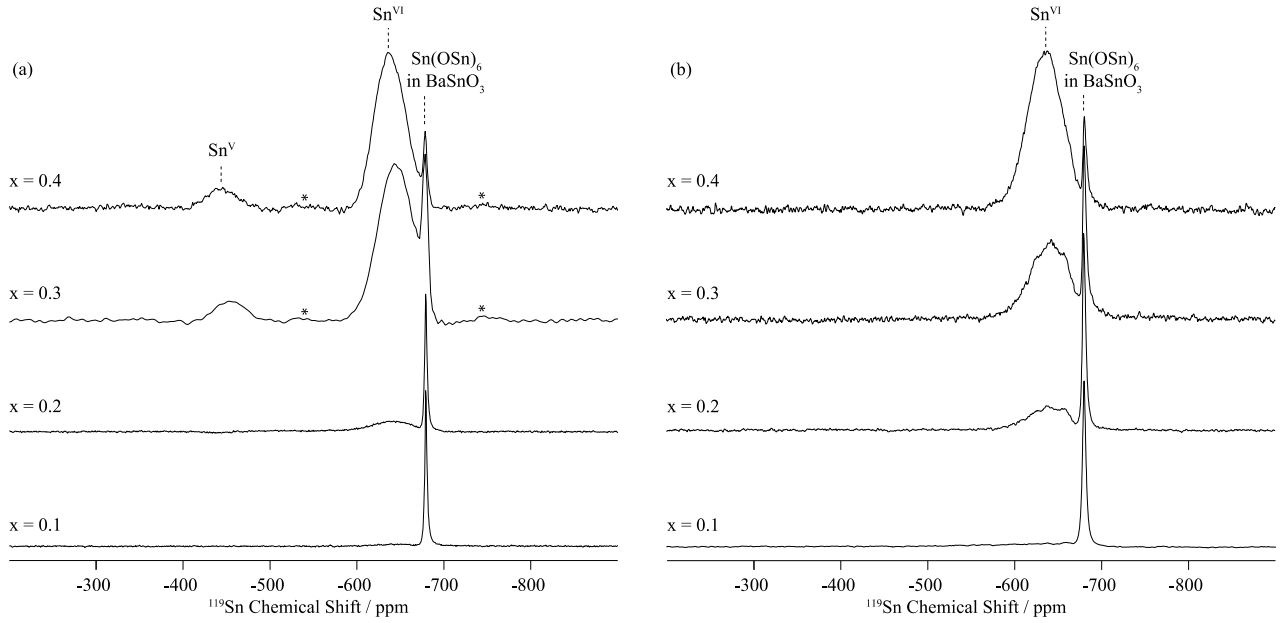

Figure 4 ^{119}Sn MAS NMR single pulse spectra of (a) dry $BaSn_{1-x}Sc_xO_{3-\delta}$ and (b) deuterated $BaSn_{1-x}Sc_xO_{3-\delta}$ as a function of Sc doping level x and were obtained at 11.7 T and under a MAS frequency of 20 kHz. Sn^{VI} and Sn^{V} denote six and five coordinated tin environments. Asterisks (*) indicate spinning side bands.

Table 2. Experimental ^{119}Sn, ^{45}Sc and ^{17}O NMR parameters dry $BaSnO_3$, dry $BaSn_{0.6}Sc_{0.4}O_{3-\delta}$ and deuterated $BaSn_{0.6}Sc_{0.4}O_{3-\delta}$.[a]

Site	Environment	δ_{iso} / ppm	C_Q / MHz	η_Q
		dry $BaSnO_3$		
Sn	$\mathbf{Sn}^{VI}(OSn)_6$	- 679	-[b]	
Sc		-[b]		
O[c]	Sn^{VI}-**O**-Sn^{VI}	152	6.1	0.0
		dry $BaSn_{0.6}Sc_{0.4}O_{3-\delta}$		
Sn	$\mathbf{Sn}^{VI}(OSn)_6$ in $BaSnO_3$	- 679(1)[31]	-[b]	
	$\mathbf{Sn}^{VI}$	- 640(10)		
	$Sn^{V}(V_O^{\bullet\bullet})$	- 450(10)		
Sc	$\mathbf{Sc}^{VI}$	120(5)	7(2)	0.7(3)
	$\mathbf{Sc}^{V}$	199(7)	20(2)	0.0(1)
O	Sn-**O**-Sn	203(5)	8(1)	-[d]
	Sn-**O**-Sc	248(10)	3(1)	-[d]
	Sn-**O**-Sc	261(8)	3(1)	-[d]
	Sc-**O**-Sc	420	5(1)	-[d]
		Hydrothermally D_2O treated $BaSn_{0.6}Sc_{0.4}O_{3-\delta}$		
Sn	$\mathbf{Sn}^{VI}(OSn)_6$ in $BaSnO_3$	- 679(1)[31]	-[b]	
	$\mathbf{Sn}^{VI}$	- 636(10)		
Sc	$\mathbf{Sc}^{VI}$	122(5)	7(2)	0.8(1)
O		-[d]		

[a] ^{45}Sc and ^{17}O NMR parameters were determined from the peak positions in the TQMAS spectra at 19.6 and 17.6 T, respectively (see SI) [25].
[b] Not applicable.
[c] Data from[32].
[d] Not measured experimentally.

3.3.2. ^{45}Sc NMR

Figures 5 and S3 (in the Supplementary Information) show the one-dimensional ^{45}Sc spectra of dry and deuterated $BaSn_{1-x}Sc_xO_{3-\delta}$ as a function of Sc doping level obtained at a high magnetic field of 19.6 T under fast MAS. The spectra of the dry samples contain a main resonance centred at around 110 ppm in addition to a much broader resonance in the 200 – 100 ppm region, which disappears upon hydrothermal D_2O treatment. Solid-state NMR spectra of quadrupolar nuclei such as ^{45}Sc (spin = 7/2) are often broad even under MAS because of residual second-order quadrupolar interactions. This can be removed by performing two-dimensional triple-quantum MAS experiment (TQMAS) [23-25] whose vertical projection along the F_1 dimension yields a one-dimensional isotropic

spectrum free of second-order broadening. Such experiments have been recorded for the dry and deuterated $BaSn_{1-x}Sc_xO_{3-\delta}$ materials (Figures 6, S4-S6) and are discussed below.

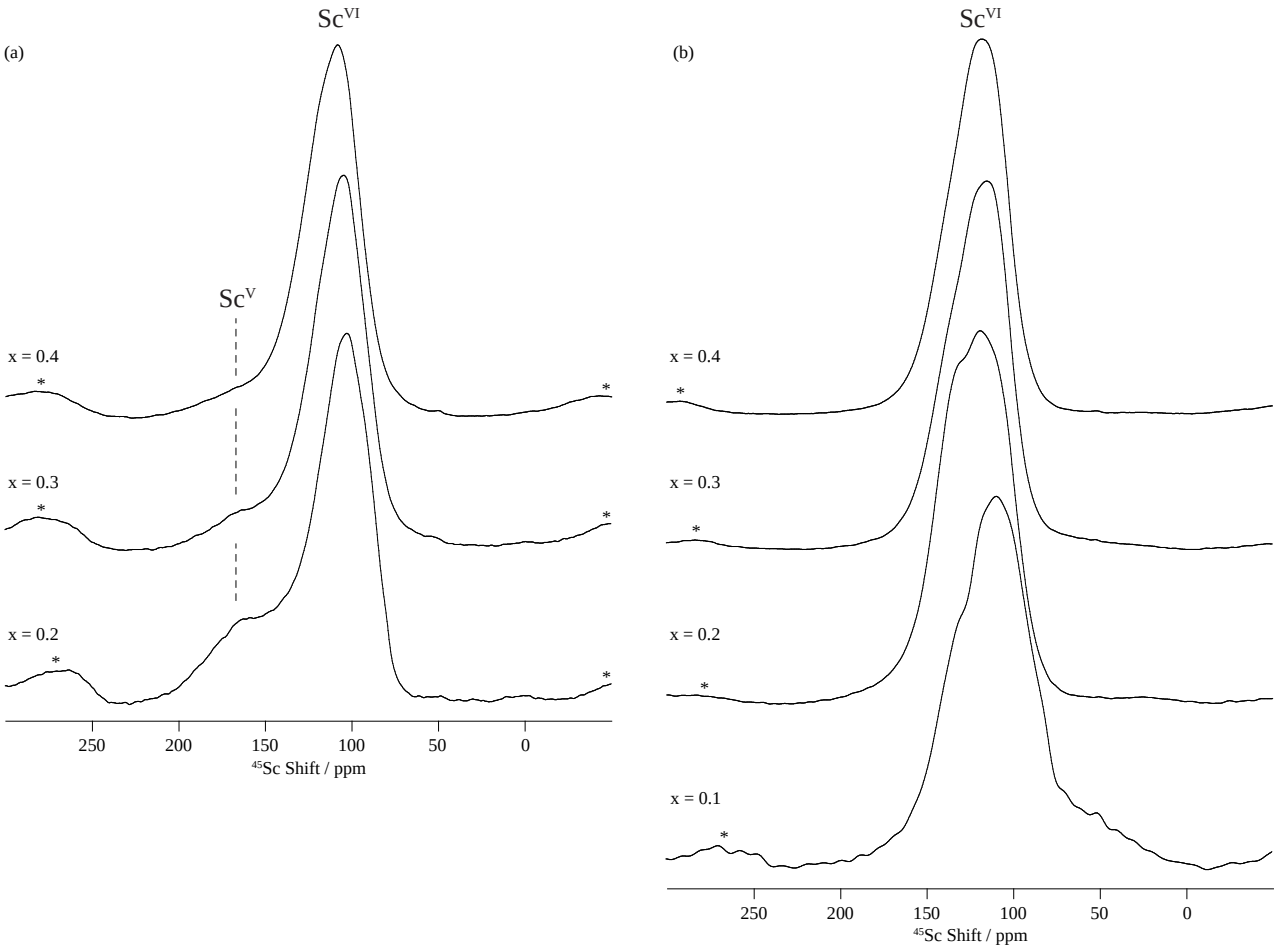

Figure 5 Central transition ^{45}Sc MAS NMR spectra of (a) dry $BaSn_{1-x}Sc_xO_{3-\delta}$ and (b) deuterated $BaSn_{1-x}Sc_xO_{3-\delta}$ as a function of Sc doping level x. The spectra were obtained at 19.6 T and under MAS frequency of 33.33 kHz. The ^{45}Sc MAS NMR spectra of dry $BaSn_{0.9}Sc_{0.1}O_{3-\delta}$ was not recorded. Sc^{VI} and Sc^{V} denote six and five coordinated scandium environments. Asterisks (*) indicate spinning side bands.

Two sets of resonances are clearly observed in the F_1 vertically projected spectra of the dry $BaSn_{0.6}Sc_{0.4}O_{3-\delta}$ sample at shifts of approximately 125 and 225 ppm (Figure 6) demonstrating the presence of two different scandium environments. Extraction of the shifts of these resonances in the horizontal F_2 dimension allow isotropic chemical shifts values of around 120 and 200 ppm to be

extracted (see Table 2) and assigned to 6- and 5-coordinated scandium environments, respectively, based on previous study by Stebbins *et al.* [34], our previous work on the $BaZr_{1-x}Sc_xO_{3-\delta}$ series [35], and Takamura *et al.*'s recent hydration study of 10% mol Sc-substituted $BaZrO_3$[36]. The 5-coordinated Sc environment which has a very large linewidth (leading to a quadrupolar coupling of around 20 MHz) is ascribed to the presence of an oxygen vacancy in the 1st coordination shell of a Sc atom.

Upon hydrothermal D_2O treatment, the oxygen vacancies are filled by protonic (deuterons) and OD defects resulting in the loss of the 5-coordinated Sc as revealed by the ^{45}Sc NMR spectra given in Figures 5b and S4-S6b. These spectra are now dominated by resonances centered at around 125 ppm and corresponding to 6-coordinated Sc only (Table 2). In fact, more than one 6-coordinated Sc environments are often visible in the ^{45}Sc MQMAS spectra of deuterated $BaSn_{1-x}Sc_xO_{3-\delta}$, and are assigned to ScO_6 (as in the dry samples) and ScO_5(OD) environments (i.e. 6-coordinated scandium in the vicinity of a protonic defect).

Note that the Sc_2O_3 impurity seen by NPD was not observed by ^{45}Sc NMR of dry $BaSn_{0.6}Sc_{0.4}O_{3-\delta}$ (Figure 6a). This is attributed to the very small amount of Sc_2O_3 (1.11 %, Table 1), which is probably below the NMR detection limit, and to the fact that the two 6-coordinated Sc sites in Sc_2O_3 have isotropic chemical shifts of 108 and 128 ppm [34], very close to the value for 6-coordinated Sc in this sample. The lack of resolution might therefore also prevent its observation.

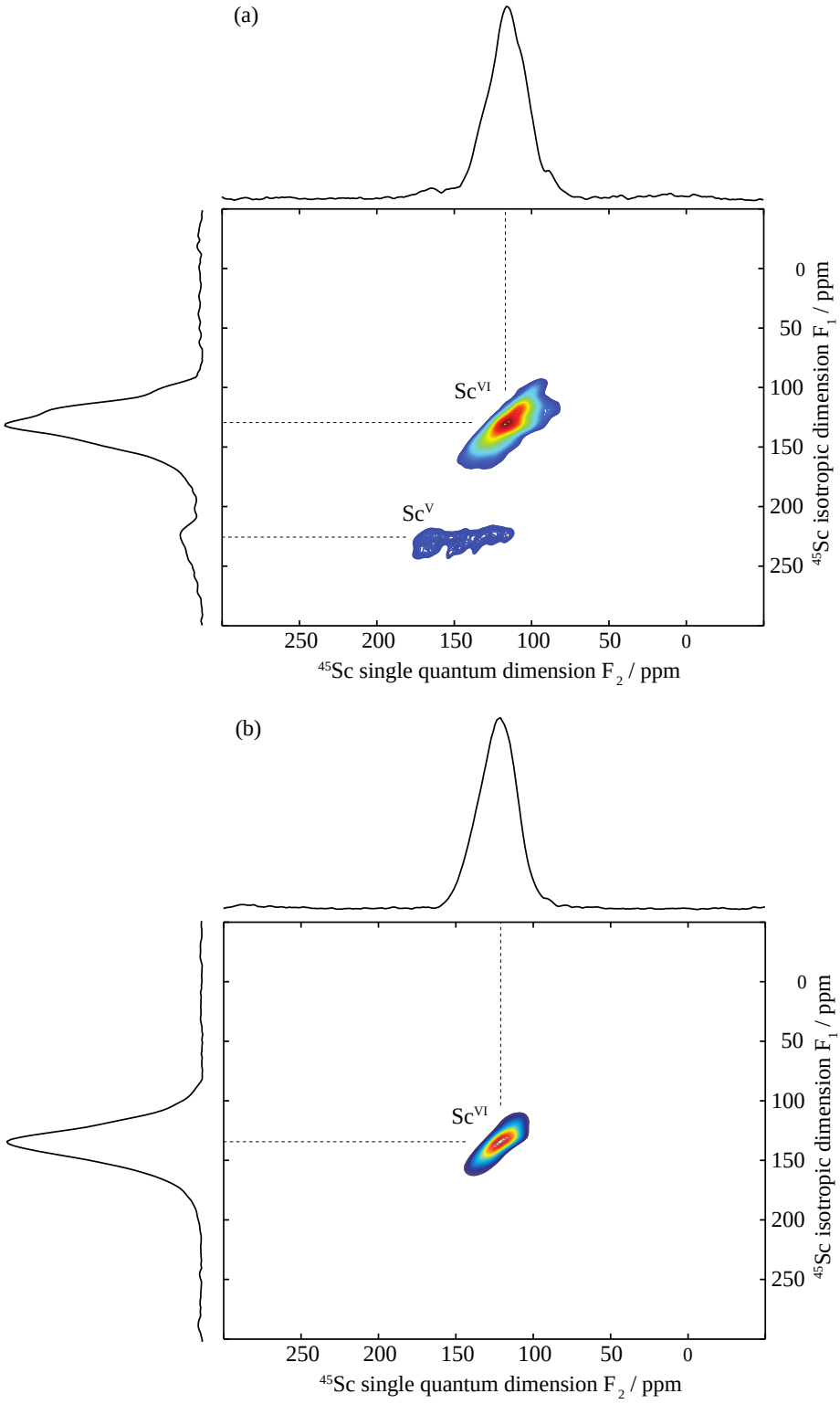

Figure 6 Two-dimensional sheared triple-quantum ^{45}Sc MAS spectra of (a) dry $BaSn_{0.6}Sc_{0.4}O_{3-\delta}$ and (b) deuterated $BaSn_{0.6}Sc_{0.4}O_{3-\delta}$ obtained at 19.6 T with a MAS frequency of 33.33 kHz. 9600 transients were accumulated for each of the 24 (for (a)) and 16 (for (b)) t_1 increments at a recycle delay of 0.4 s. Top: anisotropic skyline projection (the ^{45}Sc

MAS NMR single pulse spectra are given in Figure 5 and S3). Left: isotropic skyline projection of the TQMAS spectra. Sc^{VI} and Sc^{V} denote six and five coordinated scandium environments, respectively.

3.3.3. ^{17}O NMR

^{17}O NMR is usually very challenging due to the very low natural abundance of ^{17}O (approximately 0.037 %), often requiring isotopic enrichment. This is routinely performed in these materials via a gas – solid exchange reaction with ^{17}O enriched O_2 gas[37, 38] at elevated temperatures (see the experimental section for further details). All the one-dimensional ^{17}O MAS NMR spectra of ^{17}O enriched $BaSn_{1-x}Sc_xO_{3-\delta}$ (Figures 7 and S7) show three sets of resonances, at around 150 ppm, in the 200-300 ppm region, and centred at around 420 ppm (Table 2). The resonance around 150 ppm region consists of a single oxygen environment (see the ^{17}O MQMAS spectra, Figure S8) and is assigned to a bridging oxygen bound to two tin cations, i.e., Sn-O-Sn, based on our previous work on $BaSn_{1-x}Y_xO_{3-\delta}$[32]; this resonance is broad and may be related to the large oxygen ADP. As the Sc content is increased, this resonance remains strongly present (see Figure 7 for $BaSn_{0.6}Sc_{0.4}O_{3-\delta}$) indicating the lack of significant of Sn/Sc ordering in this material. Two peaks are clearly observed in the 200-300 ppm region, their intensities increasing with Sc concentration (relative to those for Sn-O-Sn); they are both tentatively assigned to Sc-O-Sn environments, the presence of two resonances possibly arising from Sc and Sn being five or six coordinated. A third broad resonance centred at around 420 ppm is also observed and is assigned to Sc-O-Sc oxygen environments based on previous work on the related Sc doped $BaZrO_3$ cubic perovskite.

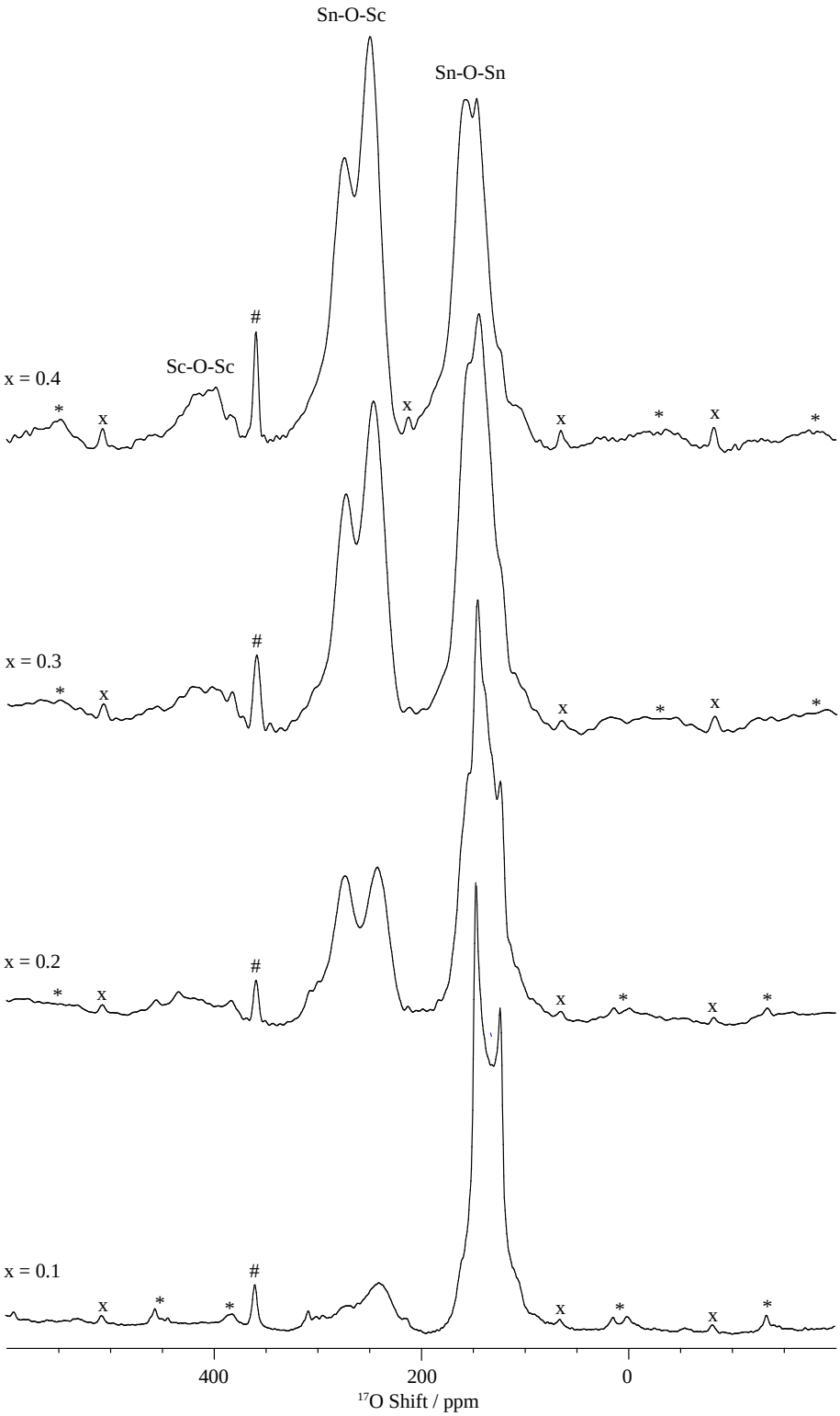

Figure 7 Central transition ^{17}O MAS NMR single pulse spectra of ^{17}O enriched $BaSn_{1-x}Sc_xO_{3-\delta}$ as a function of the Sc doping level x. The spectra were obtained at 17.6 T and under

MAS frequency of 15 kHz. The asterisks (*), dash (#) and crosses (x) denote spinning side bands, the ^{17}O signal of the ZrO_2 rotor and its spinning side bands, respectively.

3.4. Impedance Spectroscopy

Figure 8 shows the complex plane plot of the pre-hydrated $BaSn_{0.6}Sc_{0.4}O_{3-\delta}$ sample on heating at 100 °C in dry Ar. Two times constants are observed, including one in the high frequency region near the origin; the data is modelled using two (RQ) elements, representing a resistor and constant phase element in parallel, connected in series. The derived capacitances were 1.17×10^{-11} F cm^{-2} and 8.14×10^{-9} F cm^{-2} consistent with bulk and grain boundary processes, respectively. The feature at the lowest frequencies is attributed to electrode processes. For the initial heating and cooling data, it was possible to separate bulk and grain boundary conductivity in this manner at temperatures below approximately 400 °C. At higher temperatures, and for the other atmospheres and thermal protocols, the data were analysed using a similar approach but here the distinction between bulk and grain boundary was not as clear and only the total conductivity (bulk + grain boundary) could be extracted.

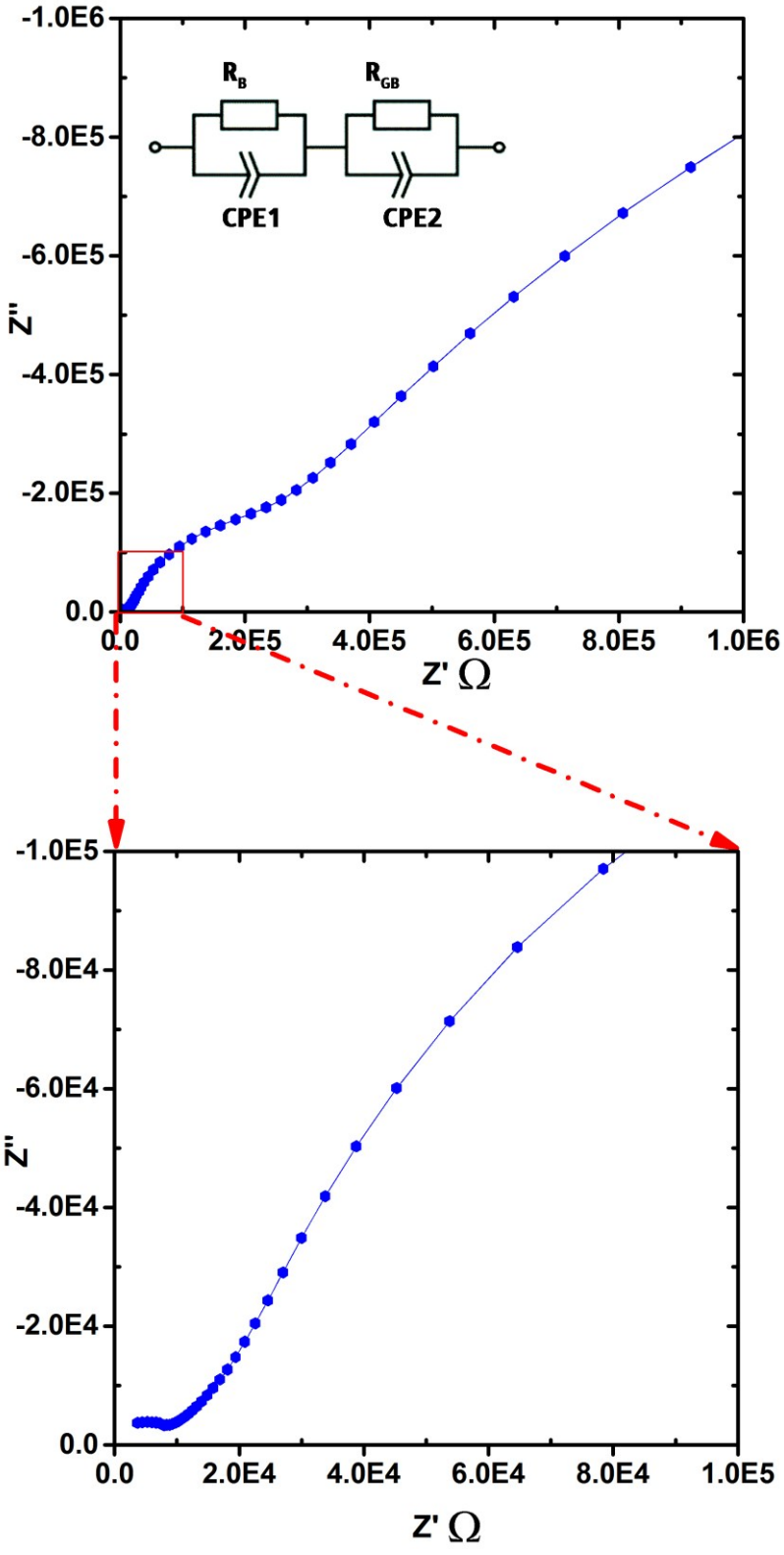

Figure 8 Typical Nyquist plot of the impedance showing the full 1 Hz-1 MHz range for pre-hydrated $BaSn_{0.6}Sc_{0.4}O_{3-\delta}$ on heating in a dry Ar atmosphere at 100 °C, the blue lines representing visual guides. A magnified view at low Z' is shown in the insert.

The conductivity data collected for $BaSn_{0.6}Sc_{0.4}O_{3-\delta}$ under Ar consisted of three regions (see Figure 9). Region I between 800 – 1000 °C has O^{2-} anions or possibly electron holes as the dominant charge carriers, while region II, between 400 – 800 °C is characteristic of the growing influence of protons and displays a characteristic plateau [39] that reflects the simultaneously varying proton concentration and proton mobility. Region III, at $T \leq 400$ °C, is dominated by proton charge carriers. Comparison of the conductivity under dry Ar vs. dry O_2 conditions reveals that the sample possesses significantly higher conductivity, approximately one order of magnitude greater, under oxidizing conditions throughout the entire temperature interval as evident in Figure 10. Conductivity under wet oxygen and above 450 °C was found, unexpectedly, to be lower than that in dry oxygen (Figure 11).

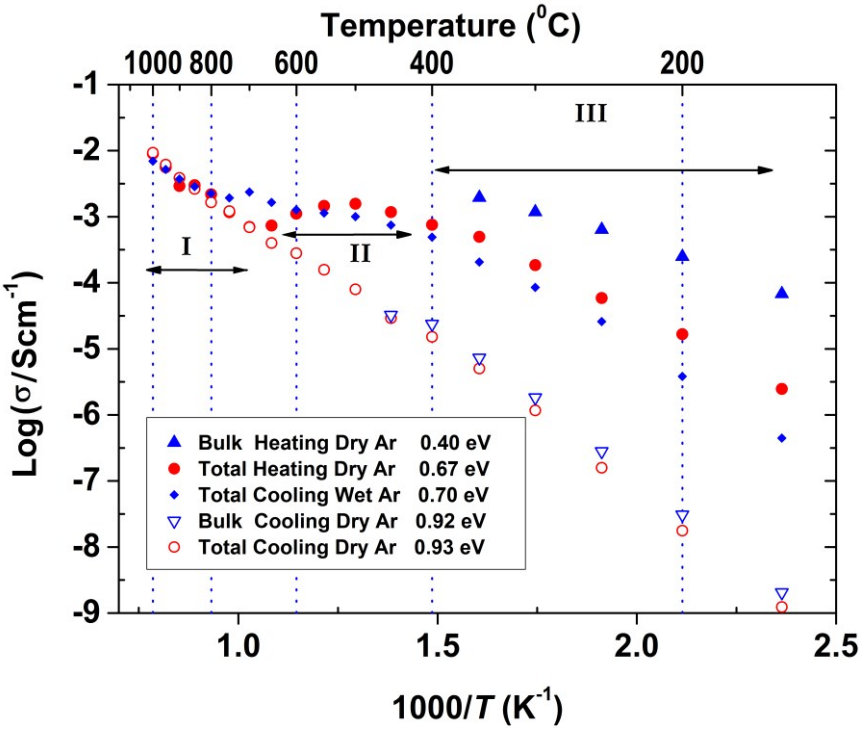

Figure 9 Arrhenius plot of the conductivity of an initially hydrated $BaSn_{0.6}Sc_{0.4}O_{3-\delta}$ sample under dry or wet Ar gas atmospheres. Three conductivity regimes (I, II and III) are observed, as highlighted, when the sample contains protons. The activation energies in the temperature regime III (below 400 °C) are indicated in the inserts.

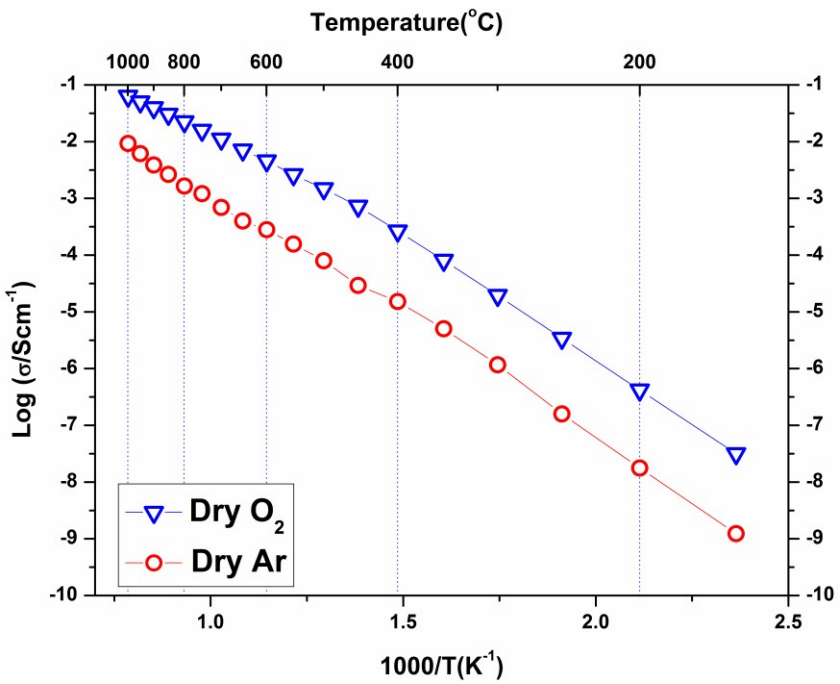

Figure 10 A comparison of the total conductivity of $BaSn_{0.6}Sc_{0.4}O_{3-\delta}$ under dry Ar gas and dry O_2 gas. The activation energies below 400 °C were 0.95 eV and 0.90 eV respectively.

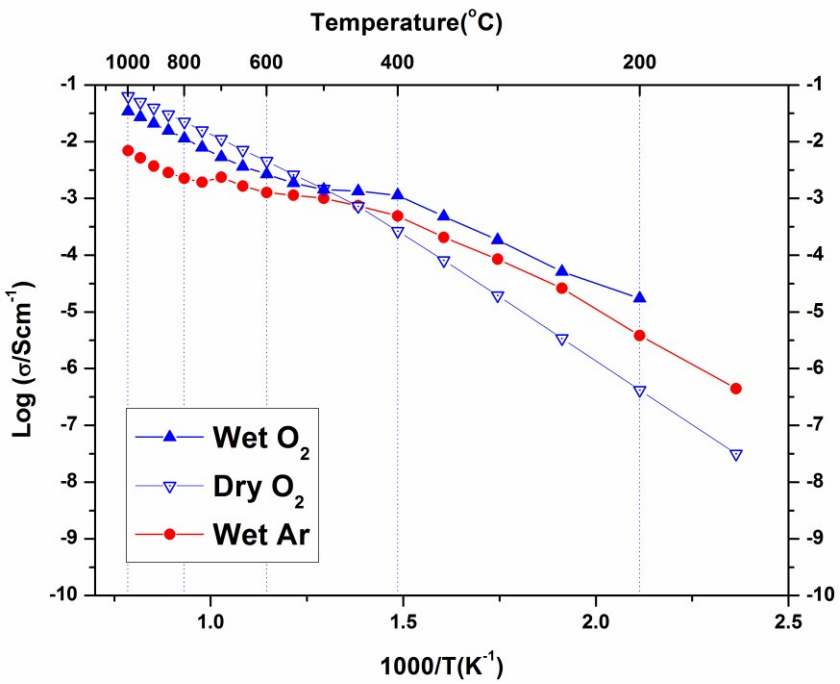

Figure 11 Total conductivity under dry O_2, wet O_2 and wet Ar gas conditions. The activation energy for the conduction processes were 0.61 eV and 0.64 eV in dry and wet O_2 respectively in the region above 600 °C while below 400 °C they were 0.90 eV and 0.63 eV respectively.

4. Discussion

4.1. Phase formation

The cell parameters extracted from the PXRD results of the as-synthesized $BaSn_{1-x}Sc_xO_{3-\delta}$ (x = 0.0, 0.1, 0.2, 0.3, 0.4) samples were found to increase with the level of Sc^{3+}dopant content. This expansion is expected as it reflects the greater ionic radius of Sc^{3+} (0.745 Å, 6-fold coordination) in comparison to Sn^{4+} (0.69 Å) [15]. Additionally, samples with dopant concentrations in the range x = 0.1 - 0.3, contained peak shoulders in their XRD patterns, which were attributed to a level of phase segregation. These results were in agreement with the ^{119}Sn NMR data which revealed the presence of sharp $Sn(OSn)_6$ environments similar to that observed in $BaSnO_3$ (Figure S2).

The cell parameters obtained in this paper for $BaSn_{1-x}Sc_xO_{3-\delta}$ are visibly lower than those reported by Wang and co-workers,[10, 11](Figure 1b) but for $BaSnO_3$ our reported value is still higher than the value of 4.1140 Å reported by both Roth et al.[40] and Cerda et al[30]. Anomalous behaviour has been reported for Sc^{3+} doped $BaZrO_3$[41] system with samples sintered at a lower temperature having a larger unit cell parameter when compared to samples sintered at higher temperatures. Hiraiwa et al.[41] demonstrate this behaviour is unique to the Sc^{3+} dopant and is contrary to the behaviour of other dopants for $BaZrO_3$. However no hypothesis exists yet to explain this behaviour.

Although $BaSn_{0.6}Sc_{0.4}O_{3-\delta}$ was initially found to be phase pure by PXRD, subsequent NPD data revealed the presence of some Sc_2O_3, and hence the possible presence of $BaSnO_3$ in the dried $BaSn_{0.6}Sc_{0.4}O_{3-\delta}$ sample. Indeed, very weak intensities, seen as shoulders on the main perovskite peaks, were visible in the NPD pattern (Figure S1) and the refined cell parameter obtained for the minor $BaSnO_3$ component of 4.11457(17) Å showed good agreement with that of the dried $BaSnO_3$ sample (a = 4.11588(2) Å). This was confirmed by the presence of the typical $Sn(OSn)_6$ resonance at – 679 ppm in the ^{119}Sn NMR data.

On hydrothermal treatment of $BaSn_{0.6}Sc_{0.4}O_{3-\delta}$ with D_2O, the minor Sc_2O_3 impurity was not observed in the NPD data, possibly indicating the complete solubility of the Sc_2O_3 into the perovskite structure is obtained under these conditions; a small signal characteristic of the local Sn environment present in $BaSnO_3$ was still observed by ^{119}Sn NMR (Figure S2). The significant difference in melting points of SnO_2 (1630 °C) and Sc_2O_3 (2485 °C) reactants suggests that different cation diffusion rates are likely to be a contributing factor for the observed sample inhomogeneity across the $BaSn_{1-x}Sc_xO_{3-\delta}$ series. The solution based synthesis approaches utilised by Wang *et al.* [10]and Buannic *et al.* [42] in the preparation of $BaSn_{1-x}Y_xO_{3-\delta}$ ($0.0 \leq x \leq 0.5$) may be expected to help overcome this issue, although we note that the presence of undoped $BaSnO_3$ was also reported for $BaSn_{0.9}Y_{0.1}O_{3-\delta}$ [42].

4.2. Deuteron site

The deuteron site of the hydrothermally D_2O treated $BaSn_{0.6}Sc_{0.4}O_{3-\delta}$ sample was successfully refined by Rietveld analysis. The deuteron atomic coordinates at the 24*k* site were $x = 0.579(3)$ and $y = 0.217(3)$ resulting in an average O-D bond distance of 0.96(1) Å, in good agreement with literature values[21, 43]. The local environment around a deuteron occupying the 24*k* site is illustrated in Figure 12 and shows three O-D interatomic distances of relevance for the proton transfer step towards acceptor oxygen ions, the closest being at 2.11(1) Å. It is clear that the local proton configuration is highly anisotropic and these results are in good agreement with experimental studies of related, highly substituted, perovskites, $BaZr_{0.5}In_{0.5}O_{2.75}$ [21] and $BaSn_{0.5}In_{0.5}O_{2.75}$ [44]. The presence of a similar next nearest O-D interaction at ~ 2.15 Å was also recently found for $BaTi_{0.5}In_{0.5}O_{2.53}(OD)_{0.44}$ from reverse Monte Carlo analysis of total scattering neutron diffraction data [45]. These findings are in line with theoretical [46-48] and experimental[49, 50] studies that revealed a clear tendency for protons to relax towards the dopant ions. The proximity of the second nearest oxygen atom indicates a tendency for enhanced hydrogen bonding interactions that will influence the proton diffusion. Whilst hydrogen bonding is expected to increase the likelihood of success for a proton transfer between neighbouring oxygen ions, the re-orientation step necessary for long range diffusion, involves breaking of the same

H-bonds. It is therefore presently unclear what the full implications of the deuteron site are for migrating protons.

Both the D_2O treated and the vacuum dried samples showed large and highly anisotropic ADPs for the oxygen site. This indicates significant static disorder of the oxygen ions as previously found [21] and it is important to stress that the refined structural models will represent a long range, time averaged, picture.

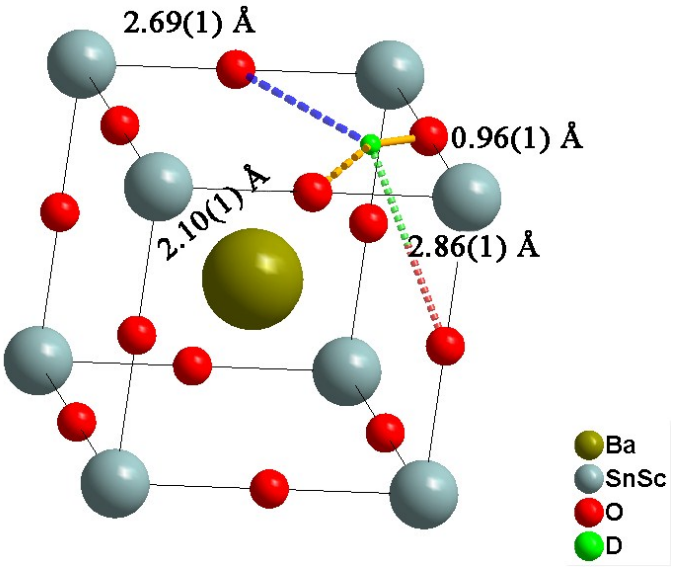

Figure 12 Illustration of the $BaSn_{0.6}Sc_{0.4}O_{2.6}(OD)_{0.4}$ unit cell showing the location of the deuteron site and its associated bond lengths to the nearest oxygen ions. The spheres represent in decreasing size Ba > Sn/Sc > O > D.

The diffraction data for the deuterated $BaSn_{0.6}Sc_{0.4}O_{2.8}$ sample revealed an increase in the cell parameter, *a*, compared to the as-prepared sample (Table 1). This lattice expansion is due to the filling of oxygen vacancies by larger hydroxyl (OD) groups and was similar in magnitude to that reported in related perovskites[39, 51]. The hydration process was also clearly reflected in the solid-state NMR data. The presence of a five-coordinate Sn and Sc peaks in the spectra of the dry $BaSn_{0.6}Sc_{0.4}O_{2.8}$

sample confirmed the existence of oxygen vacancies ($V_O^{\bullet\bullet}$) and the loss of these signals upon hydrothermal D_2O treatment confirmed their subsequent filling.

4.3. Local Sn and Sc environments

The fine structure observed for the contribution of each Y dopant cation in $Sn(OSn)_{6-z}(OY)_z$ ($0 \leq z \leq 0.4$) environment in the ^{119}Sn NMR spectra of the related $BaSn_{1-x}Y_xO_{3-\delta}$ phases [31, 32] is not observed here for $BaSn_{0.6}Sc_{0.4}O_{3-\delta}$ (Figures 4 and S2). Additionally, a signal associated with $Sn(OSn)_6$ environments persists for the highly substituted Sc sample whereas it is absent for $BaSn_{0.6}Y_{0.4}O_{2.8}$ and $BaSn_{0.5}Y_{0.5}O_{2.75}$ [32]. This suggests that there is greater disorder at the B-site and/or smaller changes in the specific local environments due to the much closer ionic radii of 6-fold coordinated Sn^{4+} (0.69 Å) and Sc^{3+} (0.745 Å vs. 6-fold Y^{3+} (0.96 Å) [15]. More importantly, the presence of noticeable concentrations of Sn-O-Sn and Sc-O-Sc environments, as revealed by ^{17}O NMR on ^{17}O enriched $BaSn_{0.6}Sc_{0.4}O_{3-\delta}$, confirms the absence of significant Sn/Sc ordering; for strict ordering and x = 0.5, only the Sc-O-Sn environment should be present, analogous to the behaviour of $BaSn_{0.5}Y_{0.5}O_{2.75}$ ($Ba_2SnYO_{5.5}$) [32]. For x < 0.5 this environment dominates, with lower concentrations of Sn-O-Sn environments being present, their concentration increasing with decreasing Sc content. For x = 0.1 and 0.2, the ratio of $Sn(OSn)_{6-n}(OSc)_n$ with n >0 to $Sn(OSn)_6$ sites is low but increases dramatically for x = 0.3 and 0.4, the amount of segregated $BaSnO_3$ being minimum for the later. There is a possibility that Sn, if hosting Sc in its vicinity, has a preference for hosting a high number of Sc, i.e. $Sn(OSn)_{6-n}(OSc)_n$ with $n \geq 3$. In such case, the concentration of $Sn(OSn)_{6-n}(OSc)_n$ with n >0 would be small for x= 0.1 and 0.2 and, combined to a broad resonance (as seen for x = 0.3 and 0.4), would yield to a very weak signal. This hypothesis is corroborated by the recurring segregation of a non-negligible amount of $BaSnO_3$, by the presence of a fair number of Sn-O-Sc bonds, and by the limited amount of Sc-O-Sc linkages as observed by ^{17}O (Fig 7) for x= 0.1 and 0.2. The greater size difference between Y^{3+} and Sn^{4+} drives a stronger tendency for ordering of the B-site cations that becomes nearly perfect with alternating Sn-O-Y-O-Sn linkages in $BaSn_{0.5}Y_{0.5}O_{2.75}$ ($Ba_2SnYO_{5.5}$) as demonstrated by

the existence a single main resonance at 259 ppm for Sn-O-Y moieties in the ^{17}O NMR spectra [32]. While some preferential cationic arrangement is possibly occurring in $BaSn_{1-x}Sc_xO_{3-\delta}$, it is not as predominant as in $BaSn_{1-x}Y_xO_{3-\delta}$.

The one-dimensional ^{45}Sc NMR spectra of dry $BaSn_{0.8}Sc_{0.2}O_{3-\delta}$ (Figure 5) reveals a clear signal for five coordinated Sc, whilst the ^{119}Sn data show no signal of 5-coordinated Sn for the x = 0.1 and 0.2 samples. Taken together, this strongly implies that oxygen vacancies are preferentially found in between or near Sc cations at low doping levels ($x \leq 0.2$). These findings agree with the results of Buannic *et al.* [35], Oikawa *et al.* [52] and [36] (for $x \leq 0.1$) on the related $BaZr_{1-x}Sc_xO_{3-\delta}$ system that suggested a tendency for the amount of 5 coordinated Sc to increase with doping level for $x \leq 0.2$. Interestingly, the one-dimensional ^{45}Sc NMR spectra reveal that the ratio of Sc^{V} to Sc^{VI} decreases as the Sc content increases above x = 0.2. A notable difference between the $BaSn_{1-x}Sc_xO_{3-\delta}$ and $BaZr_{1-x}Sc_xO_{3-\delta}$ systems is the level of dopant solubility which reaches a maximum for $BaZr_{1-x}Sc_xO_{3-\delta}$ at $x \approx 0.2$ [35], whereas the scandium incorporation level reaches $x \approx 0.35$ for the nominal x = 0.4 $BaSn_{1-x}Sc_xO_{3-\delta}$ sample based on the Sc site occupancy refined from neutron diffraction analysis for the dry material (Table 1). Buannic *et al.* [35], speculated earlier that the avoidance of energetically unfavourable Sc-O-Sc linkages, that are expected to become more numerous in systems where B-site ordering does not occur, may be a driving force for phase segregation into Sc_2O_3 and $BaZr_{1-x}Sc_xO_{3-\delta}$ with lower x. The present NMR findings for $BaSn_{0.6}Sc_{0.4}O_{3-\delta}$, showing coexistence of $Sn(OSn)_6$ and SnO_5 coordinations and low levels of ScO_5 (in comparison to the x = 0.2 sample), therefore points towards a relative abundance of Sn-$V_O^{\bullet\bullet}$-Sn local environments in comparison with a purely statistical cation and vacancy distribution. Possibly the Sn^{4+} ion is more flexible with respect to oxygen vacancies than Zr^{4+}, and this plays a role in facilitating a relatively higher scandium incorporation into the perovskite matrix.

In summary, consideration of all the NMR data reveals an intricate picture in relation to the local B-site environments. The picture that emerges is nonetheless consistent with the formation of

increasing levels of oxygen vacancies upon acceptor doping and the tendency for partial phase segregation, probably on nanometric-length scales, observed during the phase formation of the $BaSn_{1-x}Sc_xO_{3-\delta}$ series as discussed above.

4.4. Conductivity

The conductivity of $BaSn_{0.6}Sc_{0.4}O_{3-\delta}$ reveals a complex dependency on pO_2 and pH_2O. In dry, proton free, conditions the material reveals a major *p*-type contribution that is similar in magnitude to that reported recently for a related, highly acceptor doped, $BaTi_{0.5}Sc_{0.5}O_{3-\delta}$ [53]. The behaviour is also comparable to $Ba_2SnYO_{5.5}$ [9], $BaSn_{1-x}Y_xO_{3-\delta}$ [12] and $BaZr_{0.8}Y_{0.2}O_{3-\delta}$ [54] for which hole conduction dominates at high $p(O_2)$ and high T. This enhanced conductivity can be rationalised through the partial filling of oxygen vacancies resulting in the formation of mobile electron holes as described in equation 3 above.

Compared with the dry gas conditions, the conductivity under wet gas conditions (Ar or O_2), and that obtained from the initial heating run in dry Ar on the pre-hydrated sample, were significantly higher in the intermediate temperature region of 150 - 650 °C (200 - 450 °C in wet O_2) due to protons acting as the main charge carriers. Above 650 °C the conductivity obtained under wet and dry Ar were very similar as the material had probably dehydrated. This is characteristic of several related proton-conducting systems [9, 55] and reflects a transition to predominant oxide ion as protonic defects become unstable at higher T. Remarkably, at T > 450 °C under oxidizing conditions (Figure 10), the conductivity is lower under wet gas compared to dry gas, although overall it still remains significantly higher than under wet Ar. This can be rationalised on the basis of the strong *p*-type character of the material that leads to a competition between holes and protons in wet oxidising conditions. A combination of the two reactions described by equations 2 and 3 above would result in the consumption of holes in the presence of water vapour as per equation 5 below.

$$\tfrac{1}{2}H_2O_{(g)} + h^{\bullet} + O_O^x \leftrightarrows OH_O^{\bullet} + \tfrac{1}{4}O_{2\,(g)} \qquad (5)$$

This consumption of holes depletes the number of available $h^{\bullet}$ charge carriages and hence lowers the total conductivity at T > 450 °C to values below those of the dry oxygen condition. This kind of behaviour has been observed for $BaZr_{0.9-x}Pr_xGd_{0.1}O_{3-\delta}$ where highly mobile electron holes ($h^{\bullet}$) were found to dominate conductivity even to very low temperatures and in wet conditions[56]. It is clear that within the T range ~ 400 – 600 °C, $BaSn_{0.6}Sc_{0.4}O_{3-\delta}$ displays significant mixed proton and electron conduction in wet oxygen, indicating potential suitability as a cathode material for PCFCs.

Table 3 lists a summary of obtained conductivity parameters for a number of acceptor doped $BaSnO_3$ and $BaTiO_3$ systems reported in the literature. For $BaSn_{0.6}Sc_{0.4}O_{3-\delta}$, it was possible to separate a bulk contribution for the initial heating run of the pre-hydrated sample at temperatures up to 350 °C. As apparent from the impedance data shown in Figure 8 and the Arrhenius plot presented in Figure 9, the total protonic conductivity is dominated by the highly resistive grain boundaries at relatively low temperatures. The bulk proton conduction in fact reaches a very high value of ~ 2×10^{-3} S cm^{-1} at 350 °C (Figure 9). The activation energy of bulk proton conductivity of $BaSn_{0.6}Sc_{0.4}O_{3-\delta}$, estimated from the heating cycle of the pre-hydrated sample in the T range 100 to 250 °C, was 0.40(1) eV. This shows reasonable agreement with the 0.52 eV reported for both of the more lightly Sc substituted $BaSnO_3$ phases [10, 57] but is closer to the 0.38 eV and 0.34 eV reported for bulk proton conduction in $BaSn_{0.875}Y_{0.125}O_{3-\delta}$ [10] and $BaSn_{0.75}Y_{0.25}O_{3-\delta}$ [57], respectively. The bulk activation energies reported by Wang *et al.* for $BaSn_{1-x}Y_xO_{3-\delta}$ ($0.05 \leq x \leq 0.375$) [12] are approximately 0.1 eV lower than the 0.51 eV reported for bulk proton conductivity in $Ba_2YSnO_{5.5}$ [9] suggesting that the long range B-site ordering found in this phase is not beneficial to proton migration. Our present findings for $BaSn_{0.6}Sc_{0.4}O_{3-\delta}$ support this trend in as much as a low (0.40 eV) activation energy for bulk proton mobility is observed. Direct comparison of bulk activation energies is, however, not straightforward and values extracted from impedance data may also reflect partial contributions from, for example, defect formation enthalpies, dopant to proton trapping and the effects of grain boundaries. Therefore, although the trend from the data on acceptor doped $BaSnO_3$ (Table 3) seemingly supports more facile

bulk proton diffusion in disordered systems we avoid drawing wider conclusions in regards to the impact of B-site ordering on proton mobility in perovskites.

The activation energies for the total protonic conduction of $BaSn_{0.6}Sc_{0.4}O_{3-\delta}$ lie in the range 0.67-0.70 eV in wet Ar which is lower than the 0.87 eV recently reported for $BaSn_{0.875}Sc_{0.125}O_{3-\delta}$ [10], and closer to the 0.73 eV obtained for $BaSn_{0.75}Sc_{0.25}O_{3-\delta}$ [57]. The total proton conductivity of 1.07×10^{-3} S cm^{-1} obtained for $BaSn_{0.6}Sc_{0.4}O_{3-\delta}$ in wet Ar at 600 °C is similar to that of $BaIn_{0.8}Ti_{0.2}O_{2.6}$ [58] and $BaTi_{0.3}Sc_{0.7}O_{3-\delta}$ [59], and is significantly higher than that reported previously for $BaSn_{1-x}Sc_xO_{3-\delta}$ with lower scandium contents[10, 11]. This behaviour probably reflects the greater proton concentration in the more highly doped system. In general a trend of increasing proton conduction with increasing dopant concentration is also apparent from Table 3. Ultimately, however, it is the proton mobility, and understanding how it is influenced by factors such as the level of B-site cation ordering and the chemical nature of the ions, that is critical in order to obtain new materials with significantly enhanced proton conductivity.

Table 3. Comparison of conductivity parameters with literature values of acceptor doped, $BaSnO_3$ and $BaTiO_3$ perovskite systems.

Material	E_a Protonic (total) / eV	E_a Protonic (bulk) / eV	Total Conductivity (Protonic) in wet gas / S cm^{-1}	Reference
$BaSn_{0.9}In_{0.1}O_{3-\delta}$	-	0.54	1.3×10^{-3} (4 % H_2 / 96 % N_2 500 °C)	11
$BaSn_{0.875}Sc_{0.125}O_{3-\delta}$	0.87	0.52	4×10^{-4} (Ar, 500 °C)	10
$BaSn_{0.75}Sc_{0.25}O_{3-\delta}$	0.73	0.52	8×10^{-4} (Ar, 500 °C)	57
$BaSn_{0.6}Sc_{0.4}O_{3-\delta}$	0.7 - 0.67	0.40	1.07×10^{-3} (Ar, 600 °C)	This work
$BaSn_{0.9}Y_{0.1}O_{3-\delta}$	-	0.49	4×10^{-5} (4 % H_2 / 96 % N_2 500 °C)	13
$BaSn_{0.875}Y_{0.125}O_{3-\delta}$	0.72	0.38	2.3×10^{-4} (Ar, 500 °C)	10
$BaSn_{0.75}Y_{0.25}O_{3-\delta}$	0.66	0.34	7×10^{-4} (Ar, 500 °C)	12
$BaSn_{0.5}Y_{0.5}O_{2.75}$ ($Ba_2YSnO_{5.5}$ double perovskite structure)	-	0.51	1.3×10^{-3} (bulk) (N_2, 600 – 400 °C)	9
$BaTi_{0.8}Sc_{0.2}O_{3-\delta}$ (6-H hexagonal structure)	0.80	0.77	1×10^{-5} (Ar, 400 °C)	59
$BaTi_{0.5}Sc_{0.5}O_{3-\delta}$	0.46	0.22	2.89×10^{-4} (Ar, 550 °C)	60
$BaTi_{0.3}Sc_{0.7}O_{3-\delta}$	0.48	-	2×10^{-3} (Ar, 600 °C)	59
$BaTi_{0.5}In_{0.5}O_{3-\delta}$	0.48	-	2.1×10^{-4} (Ar, 500 °C)	61
$BaTi_{0.2}In_{0.8}O_{3-\delta}$	-	0.42	1.1×10^{-3} (450 - 600 °C)	58

5. Conclusions

Scandium substitution of the tin site within $BaSnO_3$ has been achieved by solid-state synthesis. Some degree of phase segregation was observed in the dry materials but it has largely disappeared in the $BaSn_{0.6}Sc_{0.4}O_{2.8}$ sample after D_2O treatment. Analysis of X-ray and neutron diffraction data has indicated an average cubic symmetry of space group $Pm\bar{3}m$ and the deuteron position was successfully located at the 24*k* site (0.579(3), 0.217(3), 0) from Rietveld analysis. ^{119}Sn

solid-state NMR revealed a series of local tin environments consistent with 6 and 5 coordinate Sn environments and $BaSnO_3$ impurities. The resonance from the 6-coordinate site is broad indicating a wide range of Sn environments differing in the number of Sn and Sc cation in the 1st B-site cation coordination shell. This behaviour is very different to the structure of $BaSn_{1-x}Y_xO_{3-\delta}$ with high concentration of yttrium, in which Y-O-Sn ordering occurs. The five-coordinated Sn is observed at high Sc doping levels ($x \geq 0.4$), confirming the presence of oxygen vacancies nearby tin. Conversely, the ^{45}Sc NMR data showed the existence of intense peaks for five-coordinated Sc, the relative fraction of five to six-coordinated Sc increasing with decreasing Sc content, suggesting preferential trapping of oxygen vacancies in between or near Sc cations at lower Sc concentrations. For all compositions, the five coordinated Sc and Sn environments vanished after hydration as OH groups filled the available oxygen vacancies.

$BaSn_{0.6}Sc_{0.4}O_{3-\delta}$ was found to be predominantly a *p*-type conductor under oxidizing atmospheres with proton conduction dominating at lower temperatures. The competition between holes and protons results in a suppression of the conductivity at T > 450 °C in wet oxidizing conditions in comparison to dry oxygen. This mixed ionic and electron hole conduction means that the material could be utilized in gas separation membrane applications or cathodes of proton conducting fuel cells. The current study showed that highly scandium substituted $BaSnO_3$ supports very high bulk proton conductivity, comparable to that reported for Y-doped $BaZrO_3$ and the double perovskite $Ba_2YSnO_{5.5}$. It is suggested that further work on the material should focus on the growth of large grained samples in order to reduce grain boundary resistance, and investigate the chemical stability of the material under CO_2 atmospheres. Given the present findings, solution synthesis routes aiming to create a more homogeneous mixing of the B-site ions at the atomic level are also of potential interest.

Acknowledgements

The authors thank the Swedish Energy Agency (Energimyndigheten) and the Swedish Research Council (Vetenskapsrådet) for project funding. The UK Science and Technology Facilities Council, STFC, is thanked for allocating beam time at the ISIS Facility. The National High Magnetic Field Laboratory is supported through the National Science Foundation Cooperative Agreement (DMR-0084173) and by the State of Florida. L.B., F.B. and C.P.G. thank the NSF via grant DMR0804737 and NYSTAR for support. F.B. also thanks the EU Marie Curie actions FP7 for an International Incoming fellowship (grant *no* 275212) and the University of Liverpool for funding. C.P.G. thanks the European Research Council for an Advanced Fellowship. We thank Dr. Boris Itin for technical assistance with the NMR measurements at 17.6 T at New York Structural Biology Center, New York City, NY.

Supporting Information available

Rietveld fit of dry $BaSn_{0.6}Sc_{0.4}O_{3-\delta}$ sample (Figure S1). ^{119}Sn (Figure S2), ^{45}Sc (Figures S3-S6) and ^{17}O (Figures S7) spectra of all materials as a function of Sc doping concentration, ^{45}Sc MQMAS of deuterated $BaSn_{0.9}Sc_{0.1}O_{3-\delta}$ (Figure S4), ^{45}Sc MQMAS of dry and deuterated $BaSn_{0.8}Sc_{0.2}O_{3-\delta}$ (Figure S5), ^{45}Sc MQMAS of dry and deuterated $BaSn_{0.7}Sc_{0.3}O_{3-\delta}$ (Figure S6), ^{17}O MQMAS of ^{17}O enriched $BaSn_{0.8}Sc_{0.2}O_{3-\delta}$ and $BaSn_{0.6}Sc_{0.4}O_{3-\delta}$ (Figure S8).

Authors' contribution

I.A, S.G.E, S.T.N conceptualized and planned the project, F.G.K, I.A synthesis of the samples, F.G.K did EIS experiments and EIS data analysed with C.S.K, F.G.K, I.A, S.T.N, S.H, S.G.E neutron data collection and structural analysis, L.B. prepared the ^{17}O enriched materials. L.B., I.H., Z.G. and F.B. carried out the NMR experiments. L.B., F.B. and C.P.G. performed analysis of the NMR data. The manuscript was written with contribution from all co-authors.

List of References

1. S. P. Jiang and Y. D. Zhen, *Solid State Ionics*, 2008, **179**, 1459-1464.
2. K. D. Kreuer, *Annual Review of Materials Research*, 2003, **33**, 333-359.
3. Y. Yamazaki, R. Hernandez-Sanchez and S. M. Haile, *Chem. Mater.*, 2009, **21**, 2755-2762.
4. E. Fabbri, D. Pergolesi and E. Traversa, *Chem. Soc. Rev.*, 2010, **39**, 4355-4369.
5. H. Iwahara, T. Esaka, H. Uchida and N. Maeda, *Solid State Ionics*, 1981, **3-4**, 359-363.
6. R. C. T. Slade, S. D. Flint and N. Singh, *Solid State Ionics*, 1995, **82**, 135-141.
7. A. Manthiram, J. F. Kuo and J. B. Goodenough, *Solid State Ionics*, 1993, **62**, 225-234.
8. T. Schober, *Solid State Ionics*, 1998, **109**, 1-11.
9. P. Murugaraj, K. D. Kreuer, T. He, T. Schober and J. Maier, *Solid State Ionics*, 1997, **98**, 1-6.
10. Y. Wang, A. Chesnaud, E. Bevillon, J. Yang and G. Dezanneau, *Int. J. Hydrogen Energy*, 2011, **36**, 7688-7695.
11. Y. Wang, A. Chesnaud, E. Bévillon, J. Xiong and J. Yang, *J. Alloys Compd.*, 2013, **555**, 395-401.
12. Y. Z. Wang, A. Chesnaud, E. Bevillon and G. Dezanneau, *Solid State Ionics*, 2012, **214**, 45-55.
13. L. P. Li and J. C. Nino, *Int. J. Hydrogen Energy*, 2013, **38**, 1598-1606.
14. É. Bévillon, J. Hermet, G. Dezanneau and G. Geneste, *J. Mater. Chem. A*, 2014, **2**, 460-471.
15. R. D. Shannon, *Acta Crystallographica Section A*, 1976, **32**, 751-767.
16. S. Hull, R. I. Smith, W. I. F. David, A. C. Hannon, J. Mayers and R. Cywinski, *Physica B: Condensed Matter*, 1992, **180-181**, 1000-1002.
17. R. B. V. D. A.C. Larson *Los Alamos National Laboratory Report*, **LAUR** 86-748.
18. B. H. Toby, *J. Appl. Crystallogr.*, 2001, **34**, 210-213.
19. H. M. Rietveld, *J. Appl. Crystallogr.*, 1969, **2**, 65-71.
20. L. B. McCusker, R. B. Von Dreele, D. E. Cox, D. Louer and P. Scardi, *J. Appl. Crystallogr.*, 1999, **32**, 36-50.
21. I. Ahmed, C. S. Knee, M. Karlsson, S. G. Eriksson, P. F. Henry, A. Matic, D. Engberg and L. Börjesson, *J. Alloys Compd.*, 2008, **450**, 103-110.
22. Z. Gan, P. L. Gor'kov, W. W. Brey, P. J. Sideris and C. P. Grey, *J Magn Reson*, 2009, **200**, 2-5.
23. L. Frydman and J. S. Harwood, *J. Am. Chem. Soc.*, 1995, **117**, 5367-5368.
24. A. Medek, J. S. Harwood and L. Frydman, *J. Am. Chem. Soc.*, 1995, **117**, 12779-12787.
25. J.-P. Amoureux and M. Pruski, in *eMagRes*, John Wiley & Sons, Ltd, 2007, DOI: 10.1002/9780470034590.emrstm0319.pub2.
26. Z. Gan and H. T. Kwak, *J Magn Reson*, 2004, **168**, 346-351.
27. J.-P. Amoureux, C. Fernandez and S. Steuernagel, *Journal of Magnetic Resonance, Series A*, 1996, **123**, 116-118.
28. J. D. van Beek, *J Magn Reson*, 2007, **187**, 19-26.
29. M. Dusek, V. Petricek and L. Palatinus, *Acta Crystallographica Section A Foundations of Crystallography*, 2006, **62**, s46-s46.
30. J. Cerda, J. Arbiol, G. Dezanneau, R. Diaz and J. R. Morante, *Sensor Actuat B-Chem*, 2002, **84**, 21-25.
31. N. J. Clayden, C. M. Dobson and A. Fern, *J. Chem. Soc., Dalton Trans.*, 1989, DOI: 10.1039/DT9890000843, 843-847.
32. L. Buannic, F. Blanc, D. S. Middlemiss and C. P. Grey, *J. Am. Chem. Soc.*, 2012, **134**, 14483-14498.
33. K. J. D. MacKenzie and M. E. Smith, *Multinuclear Solid-State Nmr of Inorganic Materials*, Elsevier, 2002.

34. N. Kim, C.-H. Hsieh and J. F. Stebbins, *Chem. Mater.*, 2006, **18**, 3855-3859.
35. L. Buannic, F. Blanc, I. Hung, Z. H. Gan and C. P. Grey, *J. Mater. Chem.*, 2010, **20**, 6322-6332.
36. I. Oikawa and H. Takamura, *Chem. Mater.*, 2015, **27**, 6660-6667.
37. N. Kim and C. P. Grey, *Science*, 2002, **297**, 1317-1320.
38. S. E. Ashbrook and M. E. Smith, *Chem. Soc. Rev.*, 2006, **35**, 718-735.
39. I. Ahmed, S. G. Eriksson, E. Ahlberg, C. S. Knee, P. Berastegui, L. G. Johansson, H. Rundlof, M. Karlsson, A. Matic, L. Borjesson and D. Engberg, *Solid State Ionics*, 2006, **177**, 1395-1403.
40. R. S. Roth, *Journal of Research of the National Bureau of Standards*, 1957, **58**, 75.
41. C. Hiraiwa, D. Han, A. Kuramitsu, A. Kuwabara, H. Takeuchi, M. Majima and T. Uda, *J. Am. Ceram. Soc.*, 2013, **96**, 879-884.
42. L. Buannic, F. Blanc, D. S. Middlemiss and C. P. Grey, *J. Am. Chem. Soc.*, 2012, **134**, 14483-14498.
43. E. Kendrick, K. S. Knight, M. S. Islam and P. R. Slater, *Solid State Ionics*, 2007, **178**, 943-949.
44. T. Ito, T. Nagasaki, K. Iwasaki, M. Yoshino, T. Matsui, N. Igawa and Y. Ishii, *Solid State Ionics*, 2007, **178**, 13-17.
45. S. T. Norberg, S. M. Rahman, S. Hull, C. S. Knee and S. G. Eriksson, *J Phys Condens Matter*, 2013, **25**, 454214.
46. M. Karlsson, M. E. Björketun, P. G. Sundell, A. Matic, G. Wahnström, D. Engberg, L. Börjesson, I. Ahmed, S. Eriksson and P. Berastegui, *Physical Review B*, 2005, **72**, 1-7.
47. C. Shi and M. Morinaga, *J. Comput. Chem.*, 2006, **27**, 711-718.
48. S. J. Stokes and M. S. Islam, *J. Mater. Chem.*, 2010, **20**, 6258-6264.
49. Y. Yamazaki, F. Blanc, Y. Okuyama, L. Buannic, J. C. Lucio-Vega, C. P. Grey and S. M. Haile, *Nat Mater*, 2013, **12**, 647-651.
50. F. Blanc, L. Sperrin, D. Lee, R. Dervisoglu, Y. Yamazaki, S. M. Haile, G. De Paepe and C. P. Grey, *J Phys Chem Lett*, 2014, **5**, 2431-2436.
51. I. Sosnowska, R. Przeniosło, W. Schäfer, W. Kockelmann, R. Hempelmann and K. Wysocki, *J. Alloys Compd.*, 2001, **328**, 226-230.
52. I. Oikawa, M. Ando, Y. Noda, K. Amezawa, H. Kiyono, T. Shimizu, M. Tansho and H. Maekawa, *Solid State Ionics*, 2011, **192**, 83-87.
53. S. M. H. Rahman, I. Ahmed, R. Haugsrud, S. G. Eriksson and C. S. Knee, *Solid State Ionics*, 2014, **255**, 140-146.
54. K. Nomura and H. Kageyama, *Solid State Ionics*, 2007, **178**, 661-665.
55. I. Ahmed, S. G. Eriksson, E. Ahlberg, C. S. Knee, H. Gotlind, L. G. Johansson, M. Karlsson, A. Matic and L. Borjesson, *Solid State Ionics*, 2007, **178**, 515-520.
56. A. Magrasó, C. Frontera, A. E. Gunnæs, A. Tarancón, D. Marrero-López, T. Norby and R. Haugsrud, *J. Power Sources*, 2011, **196**, 9141-9147.
57. Y. Wang, PhD Doctorate, Ecole Centrale Paris, Chine, 2009.
58. E. Quarez, S. Noirault, M. T. Caldes and O. Joubert, *J. Power Sources*, 2010, **195**, 1136-1141.
59. S. M. Rahman, S. T. Norberg, C. S. Knee, J. J. Biendicho, S. Hull and S. G. Eriksson, *Dalton transactions*, 2014, **43**, 15055-15064.
60. S. M. H. Rahman, I. Ahmed, R. Haugsrud, S. G. Eriksson and C. S. Knee, *Solid State Ionics*, 2014, **255**, 140-146.
61. S. M. H. Rahman, C. S. Knee, I. Ahmed, S. G. Eriksson and R. Haugsrud, *Int. J. Hydrogen Energy*, 2012, **37**, 7975-7982.

Abstract

The solid-state synthesis and structural characterisation of perovskite $BaSn_{1-x}Sc_xO_{3-\delta}$ (x = 0.0, 0.1, 0.2, 0.3, 0.4) and its corresponding hydrated ceramics are reported. Powder and neutron X-ray diffractions reveal the presence of cubic perovskites (space group $Pm\bar{3}m$) with an increasing cell parameter as a function of scandium concentration along with some indication of phase segregation. ^{119}Sn and ^{45}Sc solid-state NMR spectroscopy data highlight the existence of oxygen vacancies in the dry materials, and their filling upon hydrothermal treatment with D_2O. It also indicates that the Sn^{4+} and Sc^{3+} local distribution at the B-site of the perovskite is inhomogeneous and suggests that the oxygen vacancies are located in the scandium dopant coordination shell at low concentrations ($x \leq 0.2$) and in the tin coordination shell at high concentrations ($x \geq 0.3$). ^{17}O NMR spectra on ^{17}O enriched $BaSn_{1-x}Sc_xO_{3-\delta}$ materials show the existence of Sn-O-Sn, Sn-O-Sc and Sc-O-Sc bridging oxygen environments. Further room temperature neutron powder diffraction study on deuterated $BaSn_{0.6}Sc_{0.4}O_{3-\delta}$ refines the deuteron position at the 24*k* crystallographic site (x, y, 0) with x = 0.579(3) and y = 0.217(3) which leads to an O-D bond distance of 0.96(1) Å and suggests tilting of the proton towards the next nearest oxygen. Proton conduction was found to dominate in wet argon below 700 °C with total conductivity values in the range 1.8×10^{-4} to 1.1×10^{-3} S cm^{-1} between 300 and 600 °C. Electron holes govern the conduction process in dry oxidizing conditions, whilst in wet oxygen they compete with protonic defects leading to a wide mixed conduction region in the 200 to 600 °C temperature region, and a suppression of the conductivity at higher temperature.

Keywords:

Proton Conducting Electrolyte, Neutron Powder Diffraction, Solid-State NMR, Deuteron Position, $BaSnO_3$, Mixed conductor

Graphical Abstract

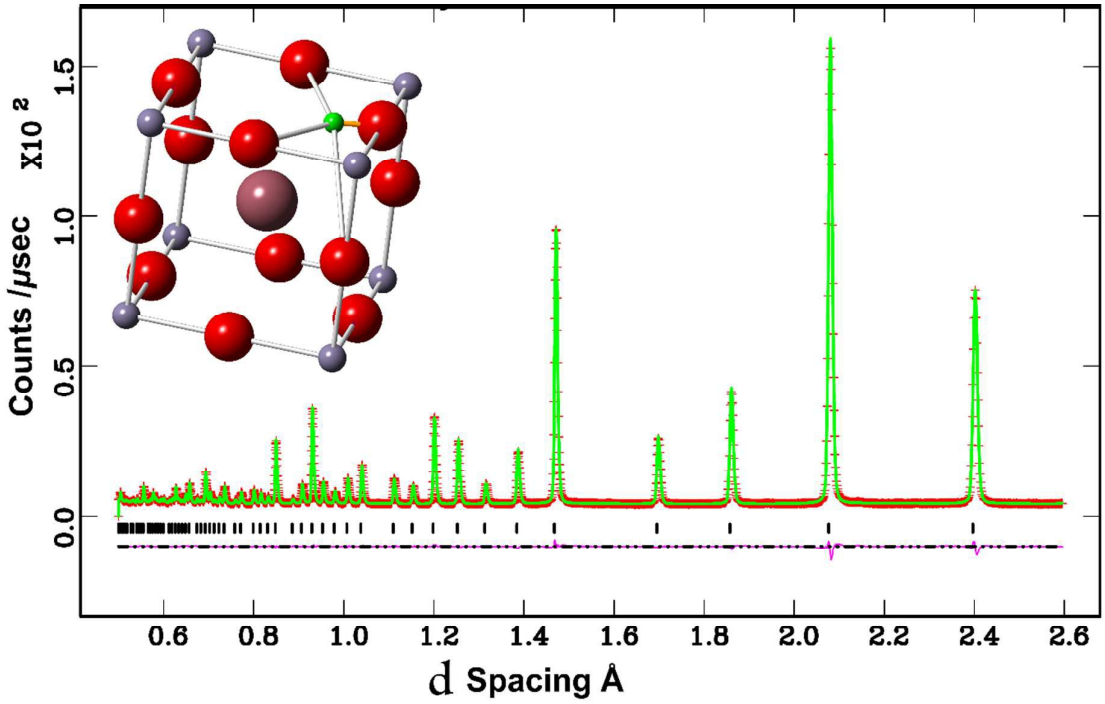

$BaSn_{0.6}Sc_{0.4}O_{3-\delta}$: Location of the proton using neutrons with insights into its high conductivity and local environment using EIS and NMR.